

# Limits on TMD Evolution From Semi-Inclusive Deep Inelastic Scattering at Moderate $Q$

C. A. Aidala,<sup>1,\*</sup> B. Field,<sup>2,†</sup> L. P. Gamberg,<sup>3,‡</sup> and T. C. Rogers<sup>4,§</sup>

<sup>1</sup>*Department of Physics,  
University of Michigan,  
Ann Arbor, MI 48109, USA*

<sup>2</sup>*Department of Physics,  
Farmingdale State College,  
2350 Broadhollow Road,  
Farmingdale, NY 11735-1021, USA*

<sup>3</sup>*Science Division,  
Penn State University-Berks,  
Reading, PA 19610, USA*

<sup>4</sup>*C.N. Yang Institute for Theoretical Physics,  
Stony Brook University,  
Stony Brook NY 11794, USA*

(Dated: January 12, 2014)

In the QCD evolution of transverse momentum dependent parton distribution and fragmentation functions, the Collins-Soper evolution kernel includes both a perturbative short-distance contribution as well as a large-distance non-perturbative, but strongly universal, contribution. In the past, global fits, based mainly on larger  $Q$  Drell-Yan-like processes, have found substantial contributions from non-perturbative regions in the Collins-Soper evolution kernel. In this article, we investigate semi-inclusive deep inelastic scattering measurements in the region of relatively small  $Q$ , of the order of a few GeV, where sensitivity to non-perturbative transverse momentum dependence may become more important or even dominate the evolution. Using recently available deep inelastic scattering data from the COMPASS experiment, we provide estimates of the regions of coordinate space that dominate in TMD processes when the hard scale is of the order of only a few GeV. We find that distance scales that are much larger than those commonly probed in large  $Q$  measurements become important, suggesting that the details of non-perturbative effects in TMD evolution are especially significant in the region of intermediate  $Q$ . We highlight the strongly universal nature of the non-perturbative component of evolution, and its potential to be tightly constrained by fits from a wide variety of observables that include both large and moderate  $Q$ . On this basis, we recommend detailed treatments of the non-perturbative component of the Collins-Soper evolution kernel for future TMD studies.

## I. INTRODUCTION AND MOTIVATION

This paper is intended to be part of an ongoing project dedicated to constraining the contributions from intrinsic, non-perturbative parton transverse momentum in inclusive high-energy hadronic collisions within a consistent transverse momentum dependent (TMD) factorization formalism. Efforts to improve constraints on non-perturbative input in TMD factorization are becoming increasingly relevant, both for studies of QCD bound state structure as well as for general perturbative QCD calculations of transverse momentum dependence in inclusive high energy interactions that extend to very low or zero transverse momentum. (See, for example, [1, 2] and references therein.)

The TMD factorization theorem establishes objects like TMD parton distribution functions (PDFs) and TMD fragmentation functions (FFs), which contain non-perturbative information, as universal. Constraints on PDFs and FFs, obtained from measurements or from non-perturbative calculational techniques, can be combined with perturbative calculations to produce first principles predictions for future experimental measurements. A steady accumulation of further measurements also improve the accuracy and precision of fits to the non-perturbative contributions, which then become input for increasingly precise predictions, which can in turn be tested against still further experiments. This process culminates in a repeating cycle of testing and refitting and further testing. Successful convergence toward

---

\*Electronic address: caidala@umich.edu

†Electronic address: bryan.field@farmingdale.edu

‡Electronic address: lpg10@psu.edu

§Electronic address: rogers@insti.physics.sunysb.edu

increasingly accurate predictions and more tightly constrained non-perturbative input is an important test of small- $\alpha_s$  perturbative QCD. Moreover, it justifies the interpretation of the non-perturbative TMD PDFs and TMD FFs as descriptions of truly intrinsic bound state properties of the colliding hadrons, and relates them to fundamental quark and gluon degrees of freedom. In this regard, the situation with TMD functions closely mirrors that of standard collinear factorization, wherein the intrinsic non-perturbative collinear properties of the colliding hadrons are encoded in the collinear PDFs.

Specifically, a TMD factorization theorem separates a transversely differential cross section into a perturbatively calculable part and several well-defined universal factors [3]. The latter are to be interpreted in terms of hadronic structure; they are objects like TMD PDFs and/or TMD FFs. (We will refer to them collectively as TMDs.) For example, the TMD factorization theorems for semi-inclusive deep inelastic scattering (SIDIS), Drell-Yan scattering (DY), and inclusive  $e^+e^-$  annihilation into back-to-back hadrons ( $e^+e^- \rightarrow H_1 + H_2 + X$ ) are schematically:

$$d\sigma_{\text{SIDIS}} = \sum_f \mathcal{H}_{f,\text{SIDIS}}(\alpha_s(\mu), \mu/Q) \otimes F_{f/H_1}(x, k_{1T}; \mu, \zeta_1) \otimes D_{H_2/f}(z, k_{2T}; \mu, \zeta_2) + Y_{\text{SIDIS}}, \quad (1)$$

$$d\sigma_{\text{DY}} = \sum_f \mathcal{H}_{f,\text{DY}}(\alpha_s(\mu), \mu/Q) \otimes F_{f/H_1}(x_1, k_{1T}; \mu, \zeta_1) \otimes F_{\bar{f}/H_2}(x_2, k_{2T}; \mu, \zeta_2) + Y_{\text{Drell-Yan}}, \quad (2)$$

$$d\sigma_{e^+e^-} = \sum_f \mathcal{H}_{f,e^+e^-}(\alpha_s(\mu), \mu/Q) \otimes D_{H_1/\bar{f}}(z_1, k_{1T}; \mu, \zeta_1) \otimes D_{H_2/f}(z_2, k_{2T}; \mu, \zeta_2) + Y_{e^+e^-}. \quad (3)$$

The first term in each equation is a generalized product of three factors. These closely resemble a literal TMD parton model description, and we will call them the ‘‘TMD terms.’’ The first factor of each TMD term is a hard part,  $\mathcal{H}(\alpha_s(\mu), \mu/Q)$ , specific to the process, with the other two factors being the universal TMD PDFs and/or FFs,  $F_{f/H_{1,2}}$  and  $D_{H_{1,2}/f}$ . The kinematical arguments,  $Q$ ,  $x_{1,2}$  and  $z_{1,2}$  have standard definitions which can be found, for example, in Ref. [3], chapter 12.14 for SIDIS, chapter 14.5 for Drell-Yan scattering, and chapter 13.2 for  $e^+e^-$  annihilation into back-to-back hadrons.

The TMDs may in general contain a mixture of both perturbative and non-perturbative contributions. But regardless of whether or not they are predominantly described by perturbative or non-perturbative behavior, they are universal, and so may be regarded as being associated with individual specific hadrons.<sup>1</sup> The last terms,  $Y_{\text{SIDIS/Drell-Yan}/e^+e^-}$ , in Eqs. (1)-(3), are corrections for the region of large transverse momentum of order  $Q$  where a description in terms of factorized TMD functions is no longer appropriate. These are called the ‘‘Y-terms.’’ Throughout this paper, we will assume that we are working with cross sections that are unpolarized and integrated over azimuthal angles.

The individual factors in Eqs. (1)-(3) contain dependence on auxiliary parameters  $\mu$ ,  $\zeta_1$  and  $\zeta_2$ , though  $\zeta_1$  and  $\zeta_2$  are not independent and are related to the physical hard scale  $Q$  via  $\sqrt{\zeta_1\zeta_2} = Q^2$ . In full QCD, the auxiliary parameters are exactly arbitrary, though to optimize the convergence properties of perturbatively calculable parts, a choice of  $\mu \sim \sqrt{\zeta_1} \sim \sqrt{\zeta_2} \sim Q$  should generally be made. From here forward we will assume that the auxiliary parameters have already been fixed at order  $Q$  so that we may rewrite Eqs. (1)-(3) in the more compact form:

$$d\sigma_{\text{SIDIS}} = \sum_f \mathcal{H}_{f,\text{SIDIS}}(\alpha_s(Q)) \otimes F_{f/H_1}(x, k_{1T}; Q) \otimes D_{H_2/f}(z, k_{2T}; Q) + Y_{\text{SIDIS}}, \quad \text{SIDIS} \quad (4)$$

$$d\sigma_{\text{DY}} = \sum_f \mathcal{H}_{f,\text{DY}}(\alpha_s(Q)) \otimes F_{f/H_1}(x_1, k_{1T}; Q) \otimes F_{\bar{f}/H_2}(x_2, k_{2T}; Q) + Y_{\text{Drell-Yan}}, \quad \text{Drell-Yan} \quad (5)$$

$$d\sigma_{e^+e^-} = \sum_f \mathcal{H}_{f,e^+e^-}(\alpha_s(Q)) \otimes D_{H_1/\bar{f}}(z_1, k_{1T}; Q) \otimes D_{H_2/f}(z_2, k_{2T}; Q) + Y_{e^+e^-}. \quad e^+e^- \rightarrow H_1 + H_2 + X \quad (6)$$

A principal goal of the TMD factorization theorem is to unify the description of all TMD-factorizable processes like Eqs. (4)-(6) (and potentially others), across all scales where perturbation theory is valid, and including the treatment of non-perturbative input. Thus, for instance, constraints on  $F_{f/H_1}(x_1, k_{1T}; Q)$  obtained from measurements using Eq. (5) may be reused in Eq. (4) to constrain  $D_{H_2/f}(z, k_{2T}; Q)$ . Likewise, constraints on  $D_{H_2/f}(z, k_{2T}; Q)$  obtained from Eq. (6) may be used in Eq. (4) to constrain  $F_{f/H_1}(x_1, k_{1T}; Q)$ . The internal consistency of such measurements tests the TMD factorization theorem and its associated universality properties and, moreover, validates the interpretation of TMD FFs and TMD PDFs as objects that can be consistently associated with intrinsic hadronic

---

<sup>1</sup> In the case of some special TMDs, like the Siverson function [4], strict universality may be relaxed in the form of a process dependent minus sign [5].

structure. Similarly, an observed dependence on the species of hadrons  $H_1$  and  $H_2$  reveals information about the intrinsic structure of the specific hadrons in terms of their elementary quark and gluon degrees of freedom.

We will work within the recent TMD-factorization theorem of Collins [3], especially chapters 10, 13 and 14, which applies at least to the classic electroweak processes in Eqs. (4)-(6). This formalism is similar to, and originates in, the earlier CSS formalism of Refs. [6–8]. The CSS formalism has been applied in particular to the construction of numerical calculations of transverse momentum distributions of Drell-Yan pairs and heavy electroweak vector bosons in high energy hadron-hadron collisions. (See Refs [9–12] and other references provided at the website [13].) Extensions of the CSS formalism were given for SIDIS in Refs. [14–16]. Though very similar in structure and implementation to the CSS formalism, there are important differences between the original CSS formalism and the TMD-factorization formalism of Ref. [3]. One complication is in how to define TMD PDFs in a way that is consistent with factorization formulas like Eqs. (4)-(6), and to identify them with the functions that are parameterized in phenomenology. Reference [17] contains a useful overview of some of the problems as they appeared approximately a decade ago. The complications outlined in Ref. [17] were mostly resolved in Ref. [3], and it is to this formulation of TMD factorization we are referring in Eqs. (4)-(6). A thorough overview of the differences between the standard CSS formalism and the formulation of Ref. [3] is beyond the scope of the current article, however, and we leave it for future work.

In addition, there are by now many other CSS-like treatments of TMD PDFs and FFs, some with important differences in details. One notable example is that of Refs. [18, 19]. Also, a TMD formalism starting from soft-collinear effective theory (SCET) considerations was derived in Ref. [20] and was shown to be equivalent, up to details, to the TMD factorization formalism of [3] in Refs. [21, 22]. A thorough comparison of different CSS-like formalisms is also beyond the scope of this article, though we expect the general conclusions to be independent of the specific formalism. We again leave a comparison of the details of different resummation and/or CSS-like approaches to future work.

For the sake of clarity, we reserve the term “TMD-factorization” to apply not just to the individual equations in Eqs. (1)-(3) and Eqs. (4)-(6), but rather to the full set of equations together with the essential properties of each factor that follow from a factorization derivation, including the infrared safety of the hard part and other perturbatively calculable quantities, the universality of the separate TMD functions, the evolution equations, and the applicability of an operator product expansion for each separate TMD function in the limit of small  $b_T$  to match to the collinear formalism. For the purpose of this article, the most important aspect of the full TMD-factorization formalism of Ref. [3] is that it is tailored to the treatment of the individual, well-defined operator definitions for the TMDs, and it maps directly onto the partonic picture displayed in the TMD terms in Eqs. (4)-(6).

In a strict parton model description, PDFs and FFs are treated literally as process-independent number densities. In real QCD, however, they acquire anomalous dependence on the hard scale  $Q$ . In both collinear and TMD factorization, scaling violations can be computed from evolution equations. Moreover, the behavior of TMD functions under evolution is closely related to the details of the derivation of factorization, provided that a factorization theorem exists. Evolution ultimately culminates in the  $Q$  dependence of the individual universal factors in Eqs. (4)-(6). Calculating and observing scaling violations is, therefore, important for testing QCD factorization in both the collinear and TMD cases.

In the collinear case, evolution is described by the well-known Dokshitzer-Gribov-Lipatov-Altarelli-Parisi (DGLAP) equations [23–25]. The TMD factorization formalism provides a different, but analogous, set of evolution equations for the TMD functions in Eqs. (4)-(6). As in the collinear case, the TMD evolution equations emerge from steps of factorization. (See Ref. [26] for a recent overview of the relationship between TMD factorization and evolution.)

An increasing number of phenomenological applications of TMD factorization now focus on separating and identifying TMDs in experimental measurements. (See, again, Refs. [1, 2].) One of the primary goals of such studies is to extract detailed information about the non-perturbative quark/gluon structure of specific hadrons. In the treatment of TMD evolution, it is therefore becoming increasingly important to incorporate, within the evolution formalism, the interpretation of TMD PDFs and FFs as actual descriptions of the quark and gluon structure of specific hadrons in formulas like Eqs. (4)-(6); that is, to use a complete TMD factorization formulation such as that in [3]. For example,  $F_{f/H_1}(x_1, \mathbf{k}_{1T}; Q)$ , should be regarded as a function specific to hadron  $H_1$  and quarks of flavor  $f$ , similar to its collinear counterpart,  $f_{f/H_1}(x_1; Q)$ . While PDFs and FFs are universal with respect to the processes under consideration, they do depend on the types of hadrons they describe. And by observing this type of dependence, one may hope to acquire information about the quark-gluon structure of specific hadronic bound states.

These points can be best highlighted with specific examples of the types of questions one hopes to address in studies that rely on TMD factorization. One may consider, for instance, the difference between valence and sea quark TMD PDFs. Chiral quark soliton models [29–32] suggest that the transverse momentum width of sea quarks in a proton

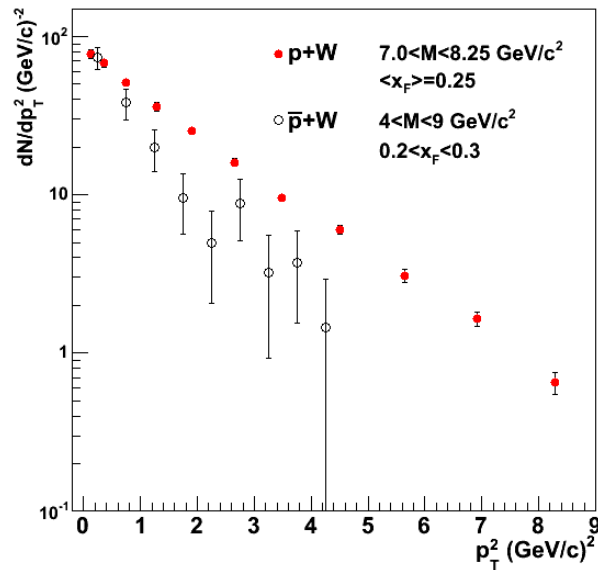


FIG. 1: Drell-Yan transverse momentum distributions in proton-Tungsten versus antiproton-Tungsten scattering. The data are from [27] and [28], respectively and have been normalized to the same value at the lowest  $P_T^2$ . The data from [27] use a beam energy of 400 GeV (27.4 GeV center-of-mass energy) while the data from [28] have a beam energy of 125 GeV (15.4 GeV center-of-mass energy).

may be as much as three times broader than that of the valance distribution [33–35].<sup>2</sup> A very direct way to test this would be to compare transverse momentum distributions for  $pA$  and  $\bar{p}A$  Drell-Yan collisions in experiments done with exactly the same kinematics, where  $A$  is a nucleus target. In the  $pA$  case, the (quark-in-proton)  $\times$  (antiquark-in- $A$ ) TMD PDF combination appears in the factorization theorem in Eq. (5) whereas in the  $\bar{p}A$  case it is the (antiquark-in-antiproton)  $\times$  (quark-in- $A$ ) TMD PDF combination that enters.<sup>3</sup> As such, the difference between transverse momentum distributions concerns the difference between sea quark versus valence quark TMD PDFs. Ideally, to see an effect, a comparison should be done with both experiments performed at exactly the same values of  $x_1$ ,  $x_2$  and  $Q$  to avoid mixing dependence on the species of the TMD PDF with variations in kinematics. At present, the closest we can find to such a comparison in existing data is for proton-Tungsten [27] and antiproton-Tungsten [28] production of Drell-Yan pairs with overlapping bins in  $Q$  and  $x_F$ . The transverse momentum distributions, normalized to the same values in the lowest  $P_T^2$  bins, are shown in Fig. 1. At first sight, the trend appears to be consistent with the behavior described in [35]. However, the range of  $Q$  for the proton-Tungsten data is cut off at a significantly larger value of  $Q$  (7 GeV) as compared with the antiproton-Tungsten data (4 GeV). Also, most of the data in Fig. 1 are at rather large  $P_T$ , while the TMD terms only account for the region of a few GeV. Therefore, the  $Y$  term is certainly needed to reliably establish any difference in the intrinsic, non-perturbative  $P_T$  dependence. Furthermore, the proton-Tungsten data are at 1.8 times the center-of-mass energy of the antiproton-Tungsten data; the proton-Tungsten data have a beam energy of 400 GeV (27.4 GeV center-of-mass energy) whereas the antiproton-Tungsten data have a beam energy of only 125 GeV (15.4 GeV center-of-mass energy). Since higher energies also lead to a broadening of the distribution, it is not possible yet to determine whether the trend actually indicates a genuine difference between intrinsic sea and valence distributions or if it is merely an artifact of kinematics or effects from large  $P_T$ . In addition, the recent study of SIDIS data from Ref. [36] in Ref. [37] does find sensitivity to the sea quark versus valence quark distributions using a collection of Gaussian fits for the low  $P_T$  TMD PDF, but finds a slightly broader distribution for sea quark TMD PDFs only when fitting data with  $Q^2 > 1.4 \text{ GeV}^2$  – see Fig. 5(a) of Ref. [37]. Making a slightly larger  $Q^2$  cut of  $Q^2 > 1.6 \text{ GeV}^2$  for the fit, the trend appears in the opposite direction – see Fig. 6(a) of Ref. [37]. Reference [37] also finds important sensitivity to quark flavor. Stronger constraints on  $x$ ,  $z$  and  $Q$  dependence of the separate (anti)proton and Tungsten TMD PDFs are needed to establish consistency across different experiments and with non-perturbative

<sup>2</sup> In interpreting the broader sea quark distribution in Ref. [34], it is important to note that the functional form of the non-perturbative behavior for sea quarks is non-Gaussian.

<sup>3</sup> Of course, the (antiquark-in-proton)  $\times$  (quark-in- $A$ ) TMD combination also appears in the  $pA$  case, but this tends to be suppressed in the kinematics of fixed-target nuclear experiments.



theoretical approaches.

Our hope is that future improved constraints on non-perturbative input, along with more data in similar experiments, will help to clarify the possible difference between valence quark versus sea quark transverse distributions in global fits. The purpose of the present paper is not to attempt to address or answer this and similar non-perturbative questions; we mention it here only to motivate the need to formulate TMD factorization as in Eqs. (4)-(6) by including, for instance, the dependence of the TMD functions like  $F_{f/H_1}(x_1, \mathbf{k}_{1T}; Q)$  on hadron species.

In order to converge toward the types of TMD factorization theorem analyses discussed in the previous paragraphs, it will be necessary to incorporate all the important elements of the TMD factorization theorem, including predictions about the non-perturbative, large-distance behavior at large  $b_T$ . A unique aspect of TMD evolution is that the kernel for the evolution itself becomes non-perturbative in the region of large transverse distances. However, one of the important predictions of the TMD factorization theorem in [3], and a central component to the analysis of TMD evolution, is that the non-perturbative contribution to evolution is totally universal, not only with respect to different processes, but also with respect to the species of hadrons involved and kinematical variables like  $x$  and  $z$ . Furthermore, the soft evolution is independent of whether the TMDs are PDFs or FFs, and is independent of whether the hadrons and/or partons are polarized.<sup>4</sup> Therefore, a parametrization of the non-perturbative evolution from the  $Q$  dependence in one observable strongly constrains the evolution of many other observables across a wide and diverse variety of different kinds of experiments and for both TMD PDFs and TMD FFs. This strong form of universality is, therefore, an important basic test of the TMD factorization theorem. It is related to the soft factors – the vacuum expectation values of Wilson loops – that are needed in the TMD definitions for consistent factorization with a minimal number of arbitrary cutoffs. As such, constraining the non-perturbative component of the evolution probes fundamental aspects of soft QCD.

In practical fitting, this means that the  $Q$  dependence for small transverse momentum must be fitted in some set of processes before it is used in other calculations. In principle, this would ideally be done for fixed values of kinematical parameters like  $x$  and  $z$  and for fixed species of external particles to avoid confounding dependence on  $Q$  with dependence on these other variables. In studies of hadron structure, it becomes especially critical to keep the species of hadron fixed in the extraction of non-perturbative evolution since the difference in structure of separate hadrons is often the main objective. An example is the comparison of proton-Tungsten and antiproton-Tungsten data sets shown in Fig. 1 and discussed above.

Data that allow for this ideal “apples-to-apples” comparison as a way to extract the non-perturbative evolution are sparse, and data for  $Q$  are usually correlated with  $x$  and  $z$ , making these studies difficult to implement in practice. Moreover, ideal implementations involve global fitting with a large quantity of diverse data making the fitting process complicated and labor intensive. However, it is important that such studies be performed if the Collins TMD factorization formalism is to be used reliably to probe universal non-perturbative aspects of quark and gluon degrees of freedom within a pQCD TMD factorization framework.

Important work in this direction includes the recent analysis in Ref. [38] which analyzes an impressively large collection of unpolarized SIDIS data, including data from HERMES [36, 39] and COMPASS [40]. Moreover, Ref. [38] does find some improvement in fitting when allowing for  $Q$  evolution (see discussion section). In Ref. [38], an example of an apples-to-apples comparison of the type described above would be the extraction of the  $x$ -dependence of the TMD PDF for a quark or anti-quark in a <sup>6</sup>LiD target from the red curves in the last row of plots in Fig. 10, such that  $Q$  and  $z$  are approximately fixed and  $x$  varies from  $9.90 \times 10^{-3}$  to  $4.42 \times 10^{-2}$ . Likewise, an extraction of  $Q$  dependence that avoids confounding TMD-evolution effects with  $x$ ,  $z$  and hadron species dependence, would be a fit of the red curves in the last column of Fig. 10 of Ref. [38] (although the two bins are immediately adjacent so that the lever arm for determining  $Q$  dependence is rather small).

We will perform such an analysis in Sect. IV of this article. Studies of SIDIS data are especially valuable for isolating  $x$  and  $z$  dependence and flavor dependence - a strategy also used in Ref. [37] which does find important flavor dependence. Drell-Yan and heavy boson production measurements with fixed energy and targets, but widely varying  $Q$ , are ideal for extracting non-perturbative components of TMD-evolution. Also,  $e^+e^-$ -annihilation experiments such as Belle [41] will also be useful for constraining the  $Q$  dependence in a true apples-to-apples analysis - see the analysis in Ref. [42].

Detailed global fits in the past, within the CSS formalism, have also found substantial effects from the non-perturbative component of the CS evolution kernel [15, 16, 43, 44], even at relatively large  $Q$  ( $Q \gtrsim 10$  GeV). See, especially, the recent discussion in Ref. [45]. Even at large  $Q$ , measurements of standard model parameters have been found to be sensitive to the non-perturbative component of evolution. For example, non-perturbative effects have been known for some time to be a relevant issue in measurements of the mass of the  $W$  boson [46], and recent

---

<sup>4</sup> The only dependence is on whether the target partons are quarks or gluons.

measurements of the  $W$  boson mass in Ref. [47] find particular sensitivity to the non-perturbative component of the CS evolution kernel.

By contrast, there are recent claims [48–50], following alternative formalisms, that a non-perturbative component to evolution is fundamentally unnecessary for studying evolution, even in regions of  $Q$  as low as  $\sim 2.0$  GeV and at almost zero transverse momentum.

The current phenomenological situation is further complicated by the observation that parametrizations obtained by extrapolating large  $Q$  fits to small  $Q$  implies suspiciously rapid evolution in the region of a few GeV, a result very clearly demonstrated in the recent work of Sun and Yuan [49, 50] – see especially Fig. 2 of Ref. [50].

To summarize, with studies of hadronic structure becoming increasingly relevant in implementations of evolution, it is important to begin to obtain a more detailed phenomenological understanding of the behavior of the non-perturbative contribution to evolution, particularly if results are to be understood in terms of a unified pQCD TMD-factorization picture. As we will frequently emphasize in this paper, this will require a careful account of the dependence on hadron species, dependence on whether the processes involve PDFs or FFs, and dependence on kinematic variables like  $x$  and  $z$ .

Semi-inclusive deep inelastic scattering experiments are particularly suited to an examination of the variation in transverse momentum distributions with relatively low  $Q$  and approximately fixed  $x$ ,  $z$  and  $Q$  [51]. The COMPASS experiment has recently released data [40] for charged hadron SIDIS measurements that are differential in all kinematical parameters and cover a range of moderately low values of  $Q$ . We will use this to study the  $Q$  dependence in the region of small  $Q$  within the same experiment and for approximately fixed  $x$ ,  $z$ . The species of hadrons in Ref. [40] is not fixed; the target is  ${}^6\text{LiD}$  while the measured final state particles include all positively (negatively) charged hadrons. Furthermore, as recently illustrated in Ref. [37], there can be significant flavor dependence in the TMD functions. However, the specific mixtures of hadrons in Ref. [40] are not varied within the experiment, so for the purpose of extracting universal  $Q$  dependence, we will take this to be a reasonable proxy for fixed hadron species. While the range in  $Q$  in Ref. [40] is too small to allow for reasonably accurate fits to the non-perturbative evolution, it is significant enough that we can use it to rule out any dramatic variations with  $Q$  that might be suggested by direct direct extrapolations from large  $Q$  fits, and to infer certain general aspects of the very large coordinate space  $Q$  dependence.

We emphasize that there is overlap between this paper and those of Sun and Yuan [49, 50], which clearly illustrate a much slower evolution in existing data from what might be expected from a direct extrapolation of large  $Q$  fits to low  $Q$ . However, while both our analysis and that of Sun-Yuan find a very soft rate of evolution in the region of moderate  $Q$ , this observation is interpreted within the contexts of different formalisms. The result is that we arrive at rather different conclusions regarding the nature and relevance of the large-distance non-perturbative region and the relationship to larger  $Q$  fits. Namely, Sun-Yuan argue that the non-perturbative component of evolution is unnecessary to study of evolution in the  $Q \sim 2.0$  GeV region whereas we find that detailed knowledge of non-perturbative evolution becomes especially important at this order of  $Q$ . Since data from lower  $Q$  are ideal for constraining the strongly universal nature of the non-perturbative evolution at large transverse sizes, we argue that it should be included in future global fits that utilize TMD factorization if a unified treatment of TMD factorization is the ultimate goal. This paper was also influenced by the recent workshop proceedings [52].

In Sect. II we review the TMD factorization formalism of Ref. [3] as it pertains to phenomenological extractions with SIDIS data. In Sects. III and IV we estimate the rate of variation in the  $P_T$ -width due to TMD evolution over the moderate  $Q$  and small  $P_T$  intervals that are observed in the SIDIS data of Ref. [40]. In Sect. V, we analyze the importance of non-perturbatively large  $b_T$  behavior, and in Sect. VI we interpret the empirically observed low  $Q$  dependence of the  $P_T$  distribution in terms of the perturbative QCD TMD factorization theorem. In Sect. VII we remark on the difference in the treatment of perturbative QCD evolution in the treatment by Collins in Ref. [3] and Sun-Yuan in Ref. [49, 50]. We discuss the overall interpretation and consequences of our observations in Sect. VIII, and offer recommendations for a way forward, with an emphasis on testing the universal and intrinsic nature of any non-perturbative hadronic structures.

## II. BRIEF REVIEW OF EVOLUTION FORMULAS

Here we briefly summarize the basic formulas of TMD factorization. For a complete derivation, we refer the reader to Ref. [3], particularly chapters 10 and 13.

The transversely differential cross section (Eq. (13.116) of Ref. [3]) for SIDIS in transverse coordinate space, corre-

sponding to Eq. (4), takes the form:

$$\begin{aligned} \frac{d\sigma}{dP_T^2} &\propto \mathcal{H}(\alpha_s(Q)) \int d^2\mathbf{b}_T e^{i\mathbf{b}_T \cdot \mathbf{P}_T} \tilde{F}_{H_1}(x, b_T; Q, Q^2) \tilde{D}_{H_2}(z, b_T; Q, Q^2) + Y_{\text{SIDIS}} \\ &\propto \text{F.T. } \tilde{F}_{H_1}(x, b_T; Q, Q^2) \tilde{D}_{H_2}(z, b_T; Q, Q^2) + Y_{\text{SIDIS}}. \end{aligned} \quad (7)$$

The two-dimensional Fourier transform is needed to convert the transverse coordinate space expression into momentum space, and we drop overall factors since, for our purposes, we are only interested in the  $P_T$ -dependence. On the second line we introduce the convenient ‘‘F.T.’’ notation, where the ‘‘F.T.’’ represents the Fourier transform and all factors not related specifically to the  $b_T$ -dependence. We will mainly be working with the coordinate space integrand in the first term in Eq. (7). We will also make the simplifying assumption of quark flavor independence, so we have dropped flavor indices; flavor dependence is easily restored in later formulae.<sup>5</sup> The scales in Eq. (7) are chosen to be  $Q$  so that the hard part,  $\mathcal{H}(\alpha_s(Q))$ , has good convergence properties. The kinematical variables  $x$ ,  $z$  and  $Q$  for SIDIS are defined in the usual way, and correspond to those of Ref. [40]. In our notation,  $P$  is the four momentum of the produced hadron,  $Q^2 = -q^2$  where  $q$  is the virtual photon momentum,  $x = Q^2/(2P_{H_1} \cdot q)$  where  $P_{H_1}$  is the incoming hadron four-momentum, and  $z = P_{H_1} \cdot P/(P_{H_1} \cdot q)$ .  $P_T$  is the transverse momentum of the produced hadron in a frame where both the incoming hadron and the virtual photon have zero transverse momentum; see Fig. 1 of Ref. [40].

The TMD functions in Eq. (1) obey a set of evolution equations which we will simply quote here for easy reference. They are the Collins-Soper (CS) equations for each TMD:

$$\frac{\partial \ln \tilde{F}(x, b_T; \mu, \zeta_1)}{\partial \ln \sqrt{\zeta_1}} = \frac{\partial \ln \tilde{D}(z, b_T; \mu, \zeta_2)}{\partial \ln \sqrt{\zeta_2}} = \tilde{K}(b_T; \mu), \quad (8)$$

and the renormalization group equations

$$\frac{d\tilde{K}(b_T; \mu)}{d \ln \mu} = -\gamma_K(\alpha_s(\mu)), \quad \text{RG CS kernel} \quad (9)$$

$$\frac{d \ln \tilde{F}(x, b_T; \mu, \zeta_1)}{d \ln \mu} = \gamma_{\text{PDF}}(\alpha_s(\mu); \zeta_1/\mu^2), \quad \text{RG TMD PDF} \quad (10)$$

$$\frac{d \ln \tilde{D}(z, b_T; \mu, \zeta_2)}{d \ln \mu} = \gamma_{\text{FF}}(\alpha_s(\mu); \zeta_2/\mu^2). \quad \text{RG TMD FF} \quad (11)$$

Again, we refer the reader to Ref. [3] for details – see especially Eqs. (13.47), (13.49), (13.50) and the discussion beginning with Sect. 13.15.4. The anomalous dimensions  $\gamma_K(g(\mu))$  and  $\gamma_F(g(\mu); \zeta_F/\mu^2)$  are perturbatively calculable, and we will keep up to order  $\alpha_s$  terms. The CS kernel,  $\tilde{K}(b_T; \mu)$ , is also perturbatively calculable as long as  $b_T \ll \sim 1/\Lambda_{\text{QCD}}$ .

Over short transverse distance scales,  $1/b_T$  becomes a legitimate hard scale, and the transverse coordinate dependence in the TMD PDFs can itself be calculated in perturbation theory. With the choice of renormalization scale  $\mu \sim 1/b_T$ ,  $\alpha_s(\sim 1/b_T)$  approaches zero for small sizes due to asymptotic freedom, thus ensuring that the small size transverse coordinate dependence is optimally calculable in perturbation theory. For very large  $b_T$ , the transverse coordinate dependence corresponds to intrinsic non-perturbative behavior associated with the hadron wave function. (In momentum space, this corresponds to the onset of effects from intrinsic bound state transverse momentum in the hadron wavefunction) There, a prescription is needed to tame the growth of  $\alpha_s(1/b_T)$  and match to a non-perturbative, large distance description of the  $b_T$ -dependence. The renormalization group scale is therefore chosen to be

$$\mu_b \equiv C_1/|\mathbf{b}_*(b_T)|, \quad (12)$$

where  $\mathbf{b}_*(b)$  is a function of  $b_T$  that equals  $b_T$  at small  $b_T$ , but freezes in the limit where  $b_T$  becomes non-perturbatively large, i.e., when  $b_T$  is larger than some fixed  $b_{\text{max}}$ . This function must obey

$$\mathbf{b}_*(b_T) = \begin{cases} \mathbf{b}_T & b_T \ll b_{\text{max}} \\ \mathbf{b}_{\text{max}} & b_T \gg b_{\text{max}}. \end{cases} \quad (13)$$

---

<sup>5</sup> See, however, Ref. [51].

The most common taming prescription is

$$\mathbf{b}_*(\mathbf{b}_T) \equiv \frac{\mathbf{b}_T}{\sqrt{1 + b_T^2/b_{\max}^2}}. \quad (14)$$

Although any function obeying Eq. (13) is consistent with both TMD factorization and the standard CSS formalism, Eq. (14) is one of the simplest choices and is the one that we will adopt in this paper. The factor  $C_1$  is an arbitrary numerical constant that can be chosen to minimize higher order corrections. It is typically fixed at  $C_1 = 2e^{-\gamma_E}$ .

To put Eq. (7) into a convenient form for perturbative calculations, we need to rewrite each TMD function evolved from the reference scale  $\mu_b$  of Eq. (12). Following Ref. [3] Eq. (13.70) (along with Eq. (13.64)) we have for the TMD FF

$$\begin{aligned} \tilde{D}_{H_2}(z, b_T; Q, Q^2) &= \tilde{D}_{H_2}(z, b_*; \mu_b, \mu_b^2) \exp \left\{ -g_2(z, b_T; b_{\max}) - g_K(b_T; b_{\max}) \ln \left( \frac{Q}{Q_0} \right) \right. \\ &\quad \left. + \ln \left( \frac{Q}{\mu_b} \right) \tilde{K}(b_*; \mu_b) + \int_{\mu_b}^Q \frac{d\mu'}{\mu'} \left[ \gamma_{\text{FF}}(\alpha_s(\mu'); 1) - \ln \left( \frac{Q}{\mu'} \right) \gamma_K(\alpha_s(\mu')) \right] \right\}. \end{aligned} \quad (15)$$

The mirror expression for the TMD PDF is

$$\begin{aligned} \tilde{F}_{H_1}(x, b_T; Q, Q^2) &= \tilde{F}_{H_1}(x, b_*; \mu_b, \mu_b^2) \exp \left\{ -g_1(x, b_T; b_{\max}) - g_K(b_T; b_{\max}) \ln \left( \frac{Q}{Q_0} \right) \right. \\ &\quad \left. + \ln \left( \frac{Q}{\mu_b} \right) \tilde{K}(b_*; \mu_b) + \int_{\mu_b}^Q \frac{d\mu'}{\mu'} \left[ \gamma_{\text{PDF}}(\alpha_s(\mu'); 1) - \ln \left( \frac{Q}{\mu'} \right) \gamma_K(\alpha_s(\mu')) \right] \right\}. \end{aligned} \quad (16)$$

The functions  $\tilde{F}_{H_1}(x, b_T; \mu_b, \mu_b^2)$  and  $\tilde{D}_{H_2}(z, b_T; \mu_b, \mu_b^2)$  now have optimal perturbative behavior at small  $b_T$ . They are calculable, via an operator product expansion, in terms of collinear PDFs and FFs and Wilson coefficients with powers of small  $\alpha_s(\mu_b)$  and perturbative coefficients that are well-behaved in the limit of  $Q \gg \Lambda_{\text{QCD}}$  (and contain no large logs of  $b_T$ ). The functions  $g_1(x, b_T; b_{\max})$ ,  $g_2(z, b_T; b_{\max})$  and  $g_K(b_T; b_{\max})$  correspond to  $g_{j/H_A}(x, b_T)$ ,  $g_{H_A/f}(z_A, b_T)$ , and  $g_K(b_T)$  in Eqs. (13.70) and (13.110) of Ref. [3]. The definition of  $g_K(b_T; b_{\max})$  is given in Eq. (13.60) of Ref. [3] and the definition of  $g_2(z, b_T)$  ( $g_{H_A/f}(z_A, b_T)$ ) is given in Eq. (13.68), and there is an exactly similar definition for  $g_1(x, b_T; b_{\max})$  ( $g_{j/H_A}(x, b_T)$ ). The functions  $g_1(x, b_T; b_{\max})$  and  $g_2(z, b_T; b_{\max})$  are specific to the type of hadron and the fragmentation function, respectively. The interpretation is that they describe the corrections needed to account for the higher orders and intrinsic non-perturbative transverse motion of the bound state partons in the limit of large  $b_T$ .<sup>6</sup>

It is important to note that, although  $g_K(b_T; b_{\max})$  is totally universal,  $g_1(x, b_T; b_{\max})$  and  $g_2(z, b_T; b_{\max})$  depend in general on the species of the incoming and outgoing hadrons respectively, as well as on the fact that one TMD is a PDF while the other is an FF, just as in the case of collinear PDFs and FFs.

Let us introduce two further definitions to simplify notation. The purpose of the present paper is not to implement a detailed perturbative treatment of the small  $b_T$ -dependence, but rather to investigate the large  $b_T$  behavior at relatively small  $Q$ . Therefore, let us define,

$$-g_{\text{PDF}}(x, b_T; b_{\max}) \equiv -g_1(x, b_T; b_{\max}) + \ln \left( \tilde{F}_{H_1}(x, b_*; \mu_b, \mu_b^2) \right), \quad (17)$$

and

$$-g_{\text{FF}}(z, b_T; b_{\max}) \equiv -g_2(z, b_T; b_{\max}) + \ln \left( \tilde{D}_{H_2}(z, b_*; \mu_b, \mu_b^2) \right). \quad (18)$$

Then, Eqs. (15)-(16) become

$$\begin{aligned} \tilde{D}_{H_2}(z, b_T; Q, Q^2) &= \exp \left\{ -g_{\text{FF}}(z, b_T; b_{\max}) - g_K(b_T; b_{\max}) \ln \left( \frac{Q}{Q_0} \right) \right. \\ &\quad \left. + \ln \left( \frac{Q}{\mu_b} \right) \tilde{K}(b_*; \mu_b) + \int_{\mu_b}^Q \frac{d\mu'}{\mu'} \left[ \gamma_{\text{FF}}(\alpha_s(\mu'); 1) - \ln \left( \frac{Q}{\mu'} \right) \gamma_K(\alpha_s(\mu')) \right] \right\}, \end{aligned} \quad (19)$$

---

<sup>6</sup> In our notation, we have included  $b_{\max}$  as an explicit auxiliary parameter in  $g_1(x, b_T; b_{\max})$ ,  $g_2(z, b_T; b_{\max})$  and  $g_K(b_T; b_{\max})$  to emphasize that these functions depend on the choice of  $b_{\max}$ .

and

$$\begin{aligned} \tilde{F}_{H_1}(x, b_T; Q, Q^2) = \exp \left\{ -g_{\text{PDF}}(x, b_T; b_{\text{max}}) - g_K(b_T; b_{\text{max}}) \ln \left( \frac{Q}{Q_0} \right) \right. \\ \left. + \ln \left( \frac{Q}{\mu_b} \right) \tilde{K}(b_*; \mu_b) + \int_{\mu_b}^Q \frac{d\mu'}{\mu'} \left[ \gamma_{\text{PDF}}(\alpha_s(\mu'); 1) - \ln \left( \frac{Q}{\mu'} \right) \gamma_K(\alpha_s(\mu')) \right] \right\}. \end{aligned} \quad (20)$$

Using the TMD PDF and FF of Eqs. (19) and (20) in Eq. (7) gives the cross section in the compact form:

$$\begin{aligned} \frac{d\sigma}{dP_T^2} \propto \text{F.T.} \exp \left\{ -g_{\text{PDF}}(x, b_T; b_{\text{max}}) - g_{\text{FF}}(z, b_T; b_{\text{max}}) - 2g_K(b_T; b_{\text{max}}) \ln \left( \frac{Q}{Q_0} \right) + \right. \\ \left. + 2 \ln \left( \frac{Q}{\mu_b} \right) \tilde{K}(b_*; \mu_b) + \int_{\mu_b}^Q \frac{d\mu'}{\mu'} \left[ \gamma_{\text{PDF}}(\alpha_s(\mu'); 1) + \gamma_{\text{FF}}(\alpha_s(\mu'); 1) - 2 \ln \left( \frac{Q}{\mu'} \right) \gamma_K(\alpha_s(\mu')) \right] \right\} \\ + Y_{\text{SIDIS}}. \end{aligned} \quad (21)$$

The functions  $g_{\text{PDF}}(x, b_T; b_{\text{max}})$  and  $g_{\text{FF}}(z, b_T; b_{\text{max}})$  parametrize the intrinsic large  $b_T$  behavior associated with the TMD PDF and the TMD fragmentation function respectively. They are independent of  $Q$ . In our notation, they also include, via the definitions in Eqs. (17)-(18), the matching to the small  $b_T$  behavior that is calculable using collinear factorization. The terms in the exponent on the second line of Eq. (21) arise from solving the evolution equations in terms of the perturbatively calculable anomalous dimensions,  $\gamma_{\text{PDF}}$ ,  $\gamma_{\text{FF}}$ ,  $\gamma_K$  and the perturbative Collins-Soper (CS) evolution kernel  $\tilde{K}(b_T; \mu)$ ; the function  $g_K(b_T; b_{\text{max}})$  on the first line is the correction to the CS kernel at large  $b_T$  which includes non-perturbative effects. Note that there is an underlying simplicity in TMD evolution in that there is a single universal function  $\tilde{K}(b_T; \mu)$  that governs the evolution of the cross section at small  $P_T$ , though in Eq. (21) it has been split into three parts: the terms involving  $\gamma_K(\alpha_s(\mu'))$ ,  $\tilde{K}(b_*; \mu_b)$ , and  $g_K(b_T; b_{\text{max}})$ .

It should be noted that there are multiple ways of ultimately expressing solutions to the evolution equations. The most convenient choice depends on the goals at hand, and on which particular physical phenomena one wishes to probe. We will use one example in Sect. VI.

The TMD terms in Eqs. (4)-(6) are derived using the approximation that  $P_T \ll Q$ . For an accurate calculation of the full cross section, a correction term, the  $Y$ -term, is need for the region  $P_T \sim Q$ , and this is symbolized by the last term in Eq. (21). From here forward, we will neglect the  $Y$ -term contribution and focus only on the TMD term, which remains common practice in phenomenological studies done at moderate  $Q$ . We will remark on how legitimate such an approximation is in Sect. VIII.

With the  $b_T$ -dependence of the perturbatively calculable part of Eq. (21) frozen above a certain  $b_{\text{max}}$ , the remaining evolution is described by the function  $g_K(b_T; b_{\text{max}})$ , which is totally universal and independent of  $Q$ ,  $x$ , or  $z$ .  $g_K(b_T; b_{\text{max}})$  generally contains both perturbatively calculable contributions and non-perturbative effects. By its definition, Eq. (13.60) of Ref. [3], it must vanish like a power at small  $b_T$ . Detailed studies of power corrections in Refs. [53–56] suggest that  $g_K(b_T; b_{\text{max}})$  should vanish like  $b_T^2$  (or an even power of  $b_T$ ) as  $b_T \rightarrow 0$ . See, especially, Eq. (6.2) of Ref. [54] and also the discussion around Eq. (55) of Ref. [55].

The value of  $b_{\text{max}}$ , as well as the functional form for the matching in Eq. (14), is exactly arbitrary in full QCD. In practical applications, it is preferable to choose it to be large enough to maximize the perturbative content of the calculation, while small enough that only a solidly perturbative range of  $b_T$  is included in the calculation of  $\tilde{K}(b_*; \mu_b)$ . If, on one hand,  $b_{\text{max}}$  is chosen very large, then perturbative calculations are used at large  $b_T$  where their validity is suspect. Large corrections from  $g_K(b_T; b_{\text{max}})$  would then be needed to recover the true cross section. On the other hand, if  $b_{\text{max}}$  is chosen too small, most of the work in fitting would go into reproducing results that might otherwise be accounted for by perturbation theory if  $b_{\text{max}}$  were chosen larger.

However, the formalism is set up to be neutral as to where the actual transition from perturbative to non-perturbative  $b_T$ -dependence actually occurs, and at a given order there is no distinction made between neglected higher order corrections and unavoidably non-perturbative contributions. Therefore, assuming  $Q \gg \Lambda_{\text{QCD}}$ , a desired degree of precision may be in principle achieved point-by-point in all  $b_T$  with a suitable combination of higher order calculations and constrained non-perturbative but universal input, and this remains true for any choice of  $b_{\text{max}}$ . Thus, both the traditional CSS formalism and the TMD formalism of [3] are exactly model independent in the sense that they accommodate any parametrization of non-perturbative large- $b_T$  physics.<sup>7</sup>

---

<sup>7</sup> Of course, non-perturbative physics need not be regarded as a type of model input if first principles non-perturbative calculational methods are available.

The perturbative part of the CS kernel,  $\tilde{K}(b_*; \mu_b)$ , is defined in Eq. (21) partly by the choice of  $\mathbf{b}_*(\mathbf{b}_T)$ , including the value of  $b_{\max}$ . Then all remaining information about the large  $b_T$  behavior of the CS evolution kernel, including but not limited to non-perturbative effects, is contained completely in  $g_K(b_T; b_{\max})$ . (Note that  $g_K(b_T; b_{\max})$  may also contain perturbatively calculable contributions.) As mentioned above, the cross section is exactly independent of  $b_{\max}$ . In practical applications, however, dependence on  $b_{\max}$  typically does arise due to incomplete knowledge of the exact form of  $g_K(b_T; b_{\max})$  at large  $b_T$ .

A frequently used ansatz for  $g_K(b_T; b_{\max})$  is

$$g_K(b_T; b_{\max}) = g_2(b_{\max}) \frac{1}{2} b_T^2, \quad (22)$$

where  $g_2(b_{\max})$  is a Gaussian fit parameter. This choice for  $g_K(b_T; b_{\max})$ , if positive and reasonably large, imposes a very strong Gaussian suppression of the non-perturbative regions of  $b_T$  in Eq. (21) whenever  $Q$  becomes significantly larger than  $Q_0$ . As implied by the notation,  $g_2(b_{\max})$  should be expected to take on different values depending on the choice of  $b_{\max}$ . (Indeed, if  $b_{\max}$  is changed, then the functional form of  $g_K(b_T; b_{\max})$  may also change.) For more on this point, see section VI.

The first applications of CSS evolution in the context of hadronic structure studies in spin physics were performed by Boer [57] within the original form of the CSS formalism from Refs. [6–8]. In Ref. [58], parametrizations of the TMD PDFs were constructed out of previous non-perturbative fits within the updated version of the CSS formalism of Ref. [3], and were presented in a form where the contributions to separate operator definitions of the TMD PDFs and fragmentation functions could be automatically identified. These parametrizations were constructed from non-perturbative functions that were extracted in earlier work in the old version of the CSS formalism for Drell-Yan scattering [43, 44], and were combined with fixed scale SIDIS fits at low  $Q$  that arose in the context of hadronic structure studies [59]. A direct extrapolation of the Drell-Yan fits to low  $Q$  gives evolution that is too rapid (see, again, Ref. [50], Fig. 2), and in Ref. [58] this was conjectured to be due to the role of larger  $x$  in the small  $Q$  fits, so an  $x$ -dependent function was inserted to obtain a fit that interpolated between all of the fits, within the TMD evolution formalism. (Note that Ref. [60] finds that the transverse momentum width depends significantly on  $\sqrt{s}$  as well as  $Q$ .) By adjusting the fit parameters between those of [43] and [44], a theoretical error of approximately a factor of two was estimated. Though rough, and limited by the scarcity of TMD-style fits that included evolution for non-perturbative parts, this provided a clear illustration of how actual TMD fits map to the TMD factors of the Collins TMD factorization formalism, with the TMD parametrizations themselves mapping to the operator matrix element definitions that emerge from the TMD factorization derivation.

Another direct application of the TMD evolution formalism was applied later to the Sivers function, a polarized TMD PDF important for studies of hadron structure, in Ref. [61]. Quantitative estimates of the amount of suppression in the evolution of the Sivers asymmetry were presented in Refs. [62, 63], again based on extrapolations of earlier extractions of non-perturbative parameters from Drell-Yan scattering. Boer [63] provided a treatment in the more traditional language of applications of the CSS formalism. That the non-perturbative input is based on prior extractions is crucial in this class of phenomenological studies wherein a central goal is to establish and/or test the universality of non-perturbative functions, particularly the strong universality of the non-perturbative evolution. Reference [62] found general consistency between HERMES and COMPASS data and the extrapolations from large  $Q$  fits, lending general support for the applicability of the TMD factorization formalism in the low  $Q$  region, but the data corresponded to different ranges of  $x$  and so the analysis was not totally in line with the apples-to-apples treatment described in the introduction.

It was recently illustrated very clearly in Ref. [49, 50] that the rapid evolution given by extrapolating the non-perturbative extractions from Drell-Yan at large  $Q$  is too fast to adequately account very generally for data in the region of  $Q$  of order a few GeV. Therefore, the details of the non-perturbative contribution to evolution in the region of small  $Q$  need to be reinvestigated.

To maintain consistency with the general aim of extracting properties intrinsic to specific hadrons as outlined in the introduction, we would ideally vary  $Q$  while holding  $x$ ,  $z$ , and hadron species fixed. In experiments, however, these variables are correlated, and practical fitting becomes challenging. We will appeal, in the next section, to the multi-differential COMPASS data from Ref. [40] to study the variation in the multiplicity distribution with small variations in  $Q$  and roughly fixed  $x$  and  $z$  bins within the same experiment.

### III. EMPIRICAL RATE OF EVOLUTION IN THE REGION OF MODERATE $Q$

Empirically, the SIDIS data in Ref. [40] reveal that the differential cross section as a function of  $P_T$  is reasonably well-described by a Gaussian functional form in the region of small  $P_T$  (see, e.g., Fig. 4 of Ref. [40]), with a width

that broadens very slightly with increasing  $Q$ . In this section, we will quantify this rate of change within the language of TMD evolution.

In Ref. [40], the data for hadron multiplicities are fitted using a Gaussian form,

$$\frac{d\sigma}{dP_T^2} \propto \exp \left\{ -\frac{P_T^2}{\langle P_T^2 \rangle} \right\}, \quad (23)$$

and the resulting  $\langle P_T^2 \rangle$  values are presented. Expressed in terms of the two dimensional Fourier transform from  $b_T$ -space, Eq. (23) becomes

$$\frac{d\sigma}{dP_T^2} \propto \text{F.T.} \exp \left\{ -\frac{b_T^2 \langle P_T^2 \rangle}{4} \right\}. \quad (24)$$

The parameter  $\langle P_T^2 \rangle$  is in general a function of  $x$ ,  $z$ , and  $Q$ .

Therefore, to match to the evolved formula, Eq. (21), we assume that all the terms in the exponent of Eq. (21) can be approximated as quadratic. In particular, we need a quadratic ansatz for the functions  $g_{\text{PDF}}(x, b_T; b_{\text{max}})$  and  $g_{\text{FF}}(z, b_T; b_{\text{max}})$ :

$$g_{\text{PDF}}(x, b_T; b_{\text{max}}) \propto g_{\text{FF}}(z, b_T; b_{\text{max}}) \propto b_T^2. \quad (25)$$

A note of caution is needed here because the actual behavior of  $g_{\text{PDF}}(x, b_T; b_{\text{max}})$  and  $g_{\text{FF}}(z, b_T; b_{\text{max}})$  includes singular behavior at small  $b_T$ , corresponding to the behavior at large  $P_T$ , and accounting for this properly will involve a careful treatment of the  $Y$  term. For the moderate  $Q$  range of the COMPASS data that we consider in this article, where a Gaussian fit actually provides a good description of the data, the small  $b_T$  behavior from  $g_{\text{PDF}}(x, b_T; b_{\text{max}})$  and  $g_{\text{FF}}(z, b_T; b_{\text{max}})$  is negligible. However, the details of the initial-scale treatment of  $g_{\text{PDF}}(x, b_T; b_{\text{max}})$  and  $g_{\text{FF}}(z, b_T; b_{\text{max}})$  may become important when extending to much larger  $Q$ .

A result of CS evolution is that, for the TMD term, the  $Q$ -dependence of the logarithm of the  $b_T$ -dependence is linear in  $\ln(Q)$  – see, e.g., Eq. (3.3) of Ref. [8]. Let us therefore define,

$$\tilde{\sigma}_{\text{TMD term}} \equiv \mathcal{H}(\alpha_s(Q)) \tilde{F}_{H_1}(x, b_T; Q, Q^2) \tilde{D}_{H_2}(z, b_T; Q, Q^2). \quad (26)$$

That is, it is the Fourier transform of the TMD term in Eq. (7), corresponding to  $\tilde{W}$  in Eq. (3.3) of Ref. [8]. Then,

$$\left. \frac{d \ln \tilde{\sigma}_{\text{TMD term}}}{d \ln Q^2} \right|_{b_T \text{ dep}} = \left. \tilde{K}(b_T; \mu_0) \right|_{b_T \text{ dep}}. \quad (27)$$

Importantly, the right side is independent of  $Q$ ,  $x$  and  $z$ . Still assuming that the  $Y$ -term can be neglected, and using Eq. (24), we then make the approximation that

$$\tilde{\sigma}_{\text{TMD term}} \approx \exp \left\{ -\frac{b_T^2 \langle P_T^2 \rangle}{4} \right\}. \quad (28)$$

Another note of caution is needed here because the right side of Eq. (27) includes only the TMD term's contribution to the cross section and not the  $Y$  term, while in Eq. (28) we have approximated  $\tilde{\sigma}_{\text{TMD term}}$  by the actual fit to the cross section from Eq. (24). For now we assume this to be a reasonable starting approximation. The actual  $Q$ -dependence of the cross section including the  $Y$  term will have corrections relative to what is obtained from the combination of Eq. (27) and Eq. (28).

For small  $P_T$ , the  $P_T$ -shape of the data in Ref. [40] is empirically observed to broaden slightly as  $Q$  increases, but remains quite well described by a Gaussian parametrization. (See, however, the later discussion of tail effects in Sect. V.) The evolved differential cross section obtained from Eq. (27) remains Gaussian after evolution, within the approximation above, only if the right side of Eq. (27) can be approximated as quadratic in  $b_T$  with a negative coefficient. Therefore, if the observed Gaussian shape is to be maintained as  $Q$  varies, then Eq. (24) must take the form

$$\frac{d\sigma}{dP_T^2} \propto \text{F.T.} \exp \left\{ -\frac{b_T^2}{4} \left( \langle P_T^2 \rangle_0 + 4C_{\text{evol}} \ln \left( \frac{Q_2}{Q_1} \right) \right) \right\}. \quad (29)$$

Here,  $\langle P_T^2 \rangle_0$  may depend only on  $x$  and  $z$  (it is independent of  $Q$ ) and  $C_{\text{evol}}$  is a numerical parameter that is, in principle, independent of  $x$  and  $z$ .  $Q_1$  and  $Q_2$  are initial and final hard scales.

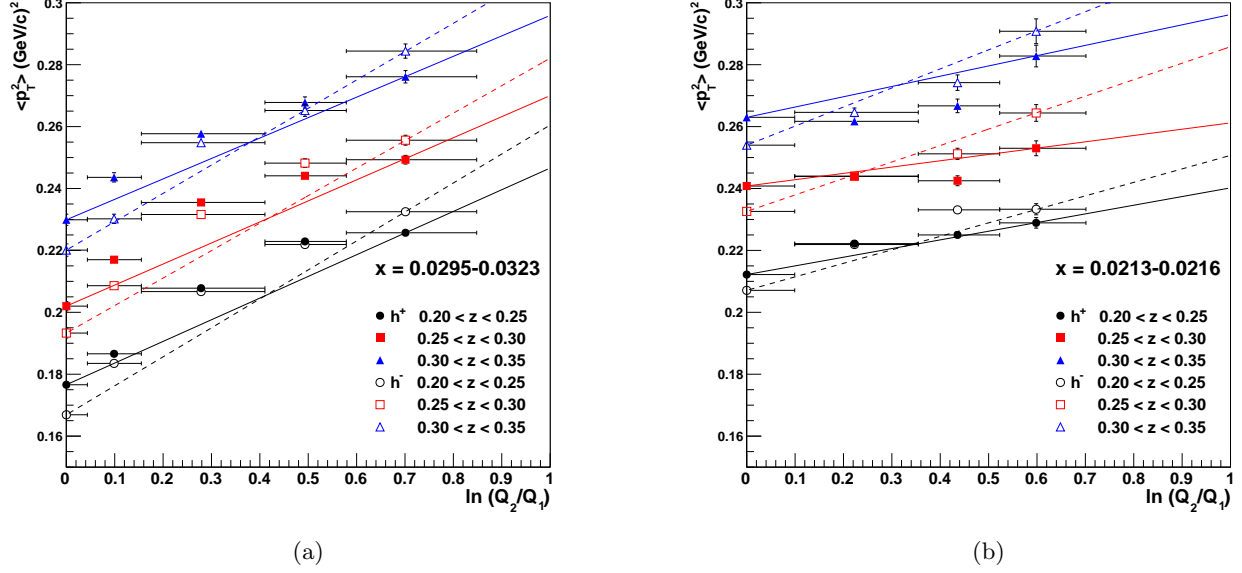


FIG. 2: Linear fits, calculated using Eq. (30), connecting low to high  $Q$  using  $C_{\text{evol}}$ . The horizontal bars show the bin widths in  $Q$ . The vertical bars are the errors of the Gaussian fits reported in Ref. [40]. Plot (a) is for  $x_{\text{bj}} = 0.0295 - 0.0323$  and plot (b) is for  $x_{\text{bj}} = 0.0213 - 0.0216$ . The solid and open points are for positive and negative produced hadrons respectively. The linear slopes are calculated using the largest and smallest  $Q_2$ ,  $Q_1$  values. (See text for details.)

If  $x$  and  $z$  are held fixed, then the variation of  $\langle P_T^2 \rangle$  with  $Q$  can be found directly from the  $b_T$ -space integrand in Eq. (29):

$$\Delta \langle P_T^2 \rangle(Q_1, Q_2) \approx 4C_{\text{evol}} \ln \left( \frac{Q_2}{Q_1} \right), \quad (30)$$

where we define

$$\Delta \langle P_T^2 \rangle(Q_1, Q_2) = \langle P_T^2 \rangle_{Q=Q_2} - \langle P_T^2 \rangle_{Q=Q_1}. \quad (31)$$

We will next use Eq. (30) to extract approximate bounds on  $C_{\text{evol}}$  from experimental results for  $\Delta \langle P_T^2 \rangle(Q_1, Q_2)$ .

The only aspect of TMD factorization that we have used so far is Eq. (27). Specifically, we have applied it to the case of the COMPASS data for the small range of  $Q$  where the  $P_T$  distribution appears to remain approximately Gaussian even after evolution to obtain Eq. (29). We do not address at this stage the question of whether  $\tilde{K}(b_T; \mu_0)$  is governed primarily by perturbative or non-perturbative  $b_T$ -dependence. While  $C_{\text{evol}}$  resembles  $g_2$  in a quadratic approximation to  $g_K(b_T; b_{\text{max}})$ , here it is meant merely to approximate the collective effect of all the  $Q$ -dependent terms in the exponent of Eq. (21), in a way consistent with Eq. (27), and it should not be identified at this stage with any specific perturbative or non-perturbative terms. Of course, perturbative contributions are not quadratic, so the quadratic ansatz for the right side of Eq. (27) is a poor one for small  $b_T$ . We will nevertheless attempt to use it to capture the general  $Q$ -dependence of the  $P_T$ -width in the vicinity of small  $Q$  variations where the data appear from [40] to be reasonably well-described by Gaussian fits. We will further analyze the reliability of such an approximation in the next few sections.

In a full treatment of evolution, there is also a  $Q$  dependence that affects only the normalization of the cross section. Since we are mainly interested in the variation in the width, we ignore any such contributions and focus only on the broadening of the Gaussian shape.

#### IV. ESTIMATES OF $C_{\text{evol}}$ FROM UNPOLARIZED SIDIS

Evolution leads to a well-known broadening of the  $P_T$  width with  $Q$  at fixed  $x$  and  $z$ . For a significant effect to be clearly observable, one must examine fixed  $x$  and  $z$  bins over sufficiently broad ranges of  $Q$ . In Ref. [40], Figs. 5



TABLE I: Estimated upper bounds on the evolution parameter  $C_{\text{evol}}$  in units of  $\text{GeV}^2$ , with positively charged produced hadrons. All values of  $Q$  are in units of  $\text{GeV}$ . See the text for an explanation of the difference between  $\langle C_{\text{evol}} \rangle$ ,  $C_{\text{evol}}^{\text{min}}$ , and  $C_{\text{evol}}^{\text{max}}$ .

| $C_{\text{evol}} = \Delta\langle P_T^2 \rangle(Q_1, Q_2) / \left( 4 \ln \left( \frac{Q_2}{Q_1} \right) \right)$ , Positively Charged Hadrons |                         |  |                         |                                 |                                   |                                |                                |  |
|--|-------------------------|--|-------------------------|---------------------------------|-----------------------------------|--------------------------------|--------------------------------|--|
| $0.2 < z < 0.25$   |                         |  |                         |                                 |                                   |                                |                                |  |
| $\sqrt{\langle Q_1^2 \rangle}, Q_1^{\text{max}}, Q_1^{\text{min}}$   | $\langle P_T^2 \rangle$ | $\sqrt{\langle Q_2^2 \rangle}, Q_2^{\text{max}}, Q_2^{\text{min}}$ | $\langle P_T^2 \rangle$ | $\langle x_{\text{bj}} \rangle$ | $\langle C_{\text{evol}} \rangle$ | $C_{\text{evol}}^{\text{min}}$ | $C_{\text{evol}}^{\text{max}}$ |  |
| 1.109, 1.225, 1.0  | 0.212                   | 2.017, 2.236, 1.871  | 0.229                   | 0.0213–0.0216                   | 0.0070                            | 0.0052                         | 0.0099                         |  |
| 1.049, 1.095, 1.0  | 0.177                   | 2.114, 2.449, 1.871  | 0.226                   | 0.0295–0.0323                   | 0.0175                            | 0.0137                         | 0.0229                         |  |
| $0.25 < z < 0.3$   |                         |  |                         |                                 |                                   |                                |                                |  |
| $\sqrt{\langle Q_1^2 \rangle}, Q_1^{\text{max}}, Q_1^{\text{min}}$   | $\langle P_T^2 \rangle$ | $\sqrt{\langle Q_2^2 \rangle}, Q_2^{\text{max}}, Q_2^{\text{min}}$ | $\langle P_T^2 \rangle$ | $\langle x_{\text{bj}} \rangle$ | $\langle C_{\text{evol}} \rangle$ | $C_{\text{evol}}^{\text{min}}$ | $C_{\text{evol}}^{\text{max}}$ |  |
| 1.109, 1.225, 1.0  | 0.241                   | 2.017, 2.236, 1.871  | 0.253                   | 0.0213–0.0216                   | 0.0051                            | 0.0040                         | 0.0071                         |  |
| 1.049, 1.095, 1.0  | 0.202                   | 2.114, 2.449, 1.871  | 0.249                   | 0.0295–0.0323                   | 0.0170                            | 0.0132                         | 0.0221                         |  |
| $0.3 < z < 0.35$   |                         |  |                         |                                 |                                   |                                |                                |  |
| $\sqrt{\langle Q_1^2 \rangle}, Q_1^{\text{max}}, Q_1^{\text{min}}$   | $\langle P_T^2 \rangle$ | $\sqrt{\langle Q_2^2 \rangle}, Q_2^{\text{max}}, Q_2^{\text{min}}$ | $\langle P_T^2 \rangle$ | $\langle x_{\text{bj}} \rangle$ | $\langle C_{\text{evol}} \rangle$ | $C_{\text{evol}}^{\text{min}}$ | $C_{\text{evol}}^{\text{max}}$ |  |
| 1.109, 1.225, 1.0  | 0.263                   | 2.017, 2.236, 1.871  | 0.283                   | 0.0213–0.0216                   | 0.0083                            | 0.0062                         | 0.0117                         |  |
| 1.049, 1.095, 1.0  | 0.230                   | 2.114, 2.449, 1.871  | 0.276                   | 0.0295–0.0323                   | 0.0165                            | 0.0130                         | 0.0216                         |  |

TABLE II: Estimated upper bounds on the evolution parameter  $C_{\text{evol}}$  in units of  $\text{GeV}^2$ , with negatively charged produced hadrons.

| $C_{\text{evol}} = \Delta\langle P_T^2 \rangle(Q_1, Q_2) / \left( 4 \ln \left( \frac{Q_2}{Q_1} \right) \right)$ , Negatively Charged Hadrons |                         |  |                         |                                 |                                   |                                |                                |  |
|--|-------------------------|--|-------------------------|---------------------------------|-----------------------------------|--------------------------------|--------------------------------|--|
| $0.2 < z < 0.25$   |                         |  |                         |                                 |                                   |                                |                                |  |
| $\sqrt{\langle Q_1^2 \rangle}, Q_1^{\text{max}}, Q_1^{\text{min}}$   | $\langle P_T^2 \rangle$ | $\sqrt{\langle Q_2^2 \rangle}, Q_2^{\text{max}}, Q_2^{\text{min}}$ | $\langle P_T^2 \rangle$ | $\langle x_{\text{bj}} \rangle$ | $\langle C_{\text{evol}} \rangle$ | $C_{\text{evol}}^{\text{min}}$ | $C_{\text{evol}}^{\text{max}}$ |  |
| 1.109, 1.225, 1.0  | 0.207                   | 2.017, 2.236, 1.871  | 0.233                   | 0.0213–0.0216                   | 0.0109                            | 0.0081                         | 0.0155                         |  |
| 1.049, 1.095, 1.0  | 0.167                   | 2.114, 2.449, 1.871  | 0.233                   | 0.0295–0.0323                   | 0.0234                            | 0.0183                         | 0.0306                         |  |
| $0.25 < z < 0.3$   |                         |  |                         |                                 |                                   |                                |                                |  |
| $\sqrt{\langle Q_1^2 \rangle}, Q_1^{\text{max}}, Q_1^{\text{min}}$   | $\langle P_T^2 \rangle$ | $\sqrt{\langle Q_2^2 \rangle}, Q_2^{\text{max}}, Q_2^{\text{min}}$ | $\langle P_T^2 \rangle$ | $\langle x_{\text{bj}} \rangle$ | $\langle C_{\text{evol}} \rangle$ | $C_{\text{evol}}^{\text{min}}$ | $C_{\text{evol}}^{\text{max}}$ |  |
| 1.109, 1.225, 1.0  | 0.233                   | 2.017, 2.236, 1.871  | 0.264                   | 0.0213–0.0216                   | 0.0133                            | 0.0100                         | 0.0188                         |  |
| 1.049, 1.095, 1.0  | 0.193                   | 2.114, 2.449, 1.871  | 0.256                   | 0.0295–0.0323                   | 0.0222                            | 0.0174                         | 0.0291                         |  |
| $0.3 < z < 0.35$   |                         |  |                         |                                 |                                   |                                |                                |  |
| $\sqrt{\langle Q_1^2 \rangle}, Q_1^{\text{max}}, Q_1^{\text{min}}$   | $\langle P_T^2 \rangle$ | $\sqrt{\langle Q_2^2 \rangle}, Q_2^{\text{max}}, Q_2^{\text{min}}$ | $\langle P_T^2 \rangle$ | $\langle x_{\text{bj}} \rangle$ | $\langle C_{\text{evol}} \rangle$ | $C_{\text{evol}}^{\text{min}}$ | $C_{\text{evol}}^{\text{max}}$ |  |
| 1.109, 1.225, 1.0  | 0.254                   | 2.017, 2.236, 1.871  | 0.291                   | 0.0213–0.0216                   | 0.0154                            | 0.0114                         | 0.0217                         |  |
| 1.049, 1.095, 1.0  | 0.220                   | 2.114, 2.449, 1.871  | 0.284                   | 0.0295–0.0323                   | 0.0229                            | 0.0179                         | 0.0300                         |  |

and 6 allow  $Q$  intervals of order  $\sim 1.0$   $\text{GeV}$  for fixed  $x$  and  $z$  bins to be identified across several bins in  $Q$ . In each panel, the fifth and sixth columns of vertical blocks correspond to fixed  $x_{\text{bj}}$  and  $z$  bins with four and five  $Q^2$ -bins, respectively. Since these give the maximum variation in  $Q$ , they are the data we will use in our analysis to obtain conservative limits on the amount of evolution at moderately small  $Q$ . In addition, we exclude data with  $z > .35$  to avoid complications with the large  $z$  region, and to be certain that we are away from significant resonance effects in the remnant. The incoming target is always  ${}^6\text{LiD}$  and the final state is inclusive in all species of charged hadrons.

Tables I, II show the results for  $C_{\text{evol}}$  from Eq. (31) for each  $x_{\text{bj}}$  and  $z$  bin. (Spreadsheets will be made available at Ref. [64].) A limitation of this analysis is the unavoidably large  $Q$  bin sizes relative to  $Q$  itself in the moderate  $Q$  region. To estimate the error from large  $Q$  bin sizes, we have therefore calculated  $C_{\text{evol}}$  using the following three

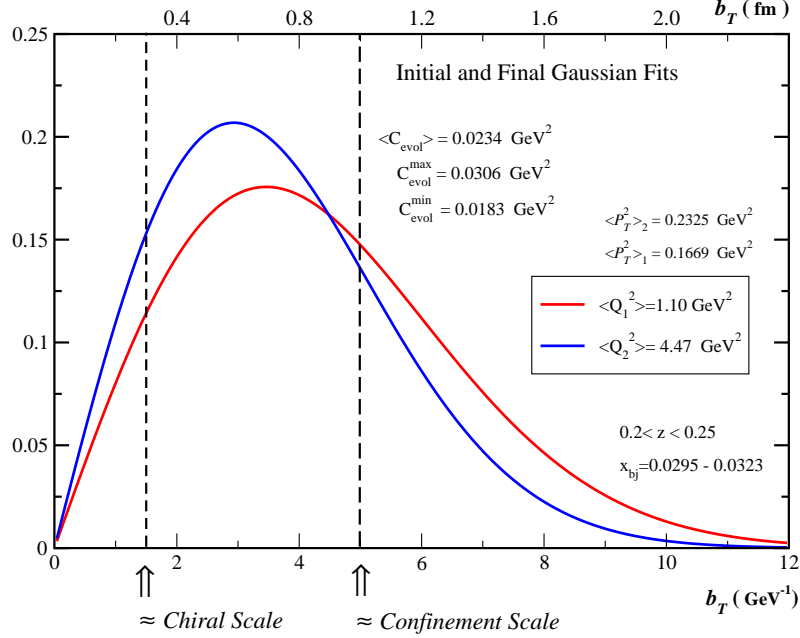


FIG. 3: Coordinate space Gaussian fits showing the largest variation in the width found in Tables I, II with a change from  $\sqrt{\langle Q_1^2 \rangle} = 1.049 \text{ GeV}$  to  $\sqrt{\langle Q_2^2 \rangle} = 2.114 \text{ GeV}$ . The precise function being plotted is Eq. (32) with the initial (red) and final (blue)  $\langle P_T^2 \rangle$  COMPASS values in Eq. (33). (See online for color.) The peak moves toward smaller values with increasing  $Q$ . These curves correspond to the first entry (smallest  $z$  bin) of Table II and the second row (largest  $x_{\text{bj}}$  bin). We have marked the approximate chiral symmetry breaking scale from Ref. [35] at  $b_T \approx 1.5 \text{ GeV}^{-1}$  and the approximate confinement scale at  $b_T \approx 5.0 \text{ GeV}^{-1}$ . Note that at the top of the graph we have also shown the horizontal axis in fm to provide a more intuitive sense of relevant size scales. Compare the dominant regions of  $b_T$  here with larger  $Q$  curves of Fig. 4 in Ref. [44].

methods: First, for  $Q_2$  and  $Q_1$  we use the average  $\langle Q^2 \rangle$  for the top and bottom  $Q^2$  bins, respectively, in Figs. 5 and 6 of Ref. [40]. The result is called  $\langle C_{\text{evol}} \rangle$  in the Tables I, II. Next, in order to obtain an estimated upper bound on the evolution we use the value of  $Q$  for the top edge of the lowest bin, called  $Q_1^{\text{max}}$  in the tables, for  $Q_1$ , and the bottom edge of the largest  $Q^2$ -bin, called  $Q_2^{\text{min}}$  in the tables, for  $Q_2$ . This will tend to underestimate  $\ln(Q_2/Q_1)$  and thus give a value for  $C_{\text{evol}}$  that is too large. The result is called  $C_{\text{evol}}^{\text{max}}$  in the tables. Similarly, to get an estimated lower bound on  $C_{\text{evol}}$ , we use the value of  $Q$  for the bottom edge of the lowest bin, called  $Q_1^{\text{min}}$  in the tables, for  $Q_1$ , and the upper edge of the largest bin, called  $Q_2^{\text{max}}$  in the tables, for  $Q_2$ . This will tend to overestimate  $\ln(Q_2/Q_1)$  and thus will tend to give a value for  $C_{\text{evol}}$  that is too small. The result is called  $C_{\text{evol}}^{\text{min}}$  in Tables I, II. Plots showing the extraction of  $C_{\text{evol}}$  are presented in Fig. 2.

Another source of error is the cutoff at  $P_T = 0.85 \text{ GeV}$  in the fits of Ref. [40], where the Gaussian description starts to break down. Variations in the precise cutoff, as well as variations in the precise functional form of fit, may affect the variation in the overall width of the distribution with  $Q$ . We will address this further in Sect. V.

The trend in Tables I, II and Fig. 2 suggests a small yet non-vanishing  $Q$ -dependence in the  $P_T$  width; the lowest value of  $C_{\text{evol}}$  is  $0.0040 \text{ GeV}^2$  and the largest value is  $0.0306 \text{ GeV}^2$ . In the next few sections, we will interpret this in the context of an analysis of the importance of contributions from different regions of  $b_T$ . We will comment further on the size of  $C_{\text{evol}}$  and its relevance to  $g_2$  in section VI.

## V. RELEVANCE OF LARGE $b_T$

In the context of applications like those outlined in the introduction, it is important to recognize that, although the  $b_T$ -dependence has both perturbative and non-perturbative contributions, the TMD factorization theorem is valid for all  $b_T$ , including  $b_T \gg 1/\Lambda_{QCD}$ , so long as  $Q$  is large enough that the expansion of  $\mathcal{H}_{f,\text{process}}(\alpha_s(Q))$  in each of Eqs. (4)-(6) is perturbatively well-behaved. TMD factorization, therefore, retains important predictive power for all  $b_T$ , regardless of how much of the  $b_T$ -dependence itself is perturbatively describable. Part of that predictive power

comes from the universality of the TMD functions, analogously to the collinear PDFs of collinear factorization, and from the very strong universality of the CS kernel, including the non-perturbative parts contained in  $g_K(b_T; b_{\max})$ .

As  $Q$  is increased, the dominant contribution to the cross section becomes localized in coordinate space around small  $b_T$  so that the non-perturbative  $b_T$  contribution becomes less important [65]. For extremely large  $Q$ , it is expected that the non-perturbative contribution can be ignored altogether. Alternatively, at moderate values of  $Q$ ,  $\alpha_s(Q)$  might be small enough that TMD factorization is completely valid, yet the  $b_T$ -dependence may still contain a large, or even dominant, non-perturbative large- $b_T$  contribution. The latter situations are ideal for extracting information about non-perturbative hadron structure in terms of elementary quark and gluon degrees of freedom within a valid pQCD TMD factorization formalism. Moreover, measurements at relatively small  $Q$  are ideal for measuring and testing the strongly universal nature of the non-perturbative scaling violations contained within  $g_K(b_T; b_{\max})$ .

Within the CSS formalism, estimates of the importance of non-perturbative  $b_T$ -dependence vary widely in the existing literature. For example, Ref. [8] estimates that the cross section can be reliably assumed to be totally insensitive to the non-perturbative region for  $Q \sim 10^8$  GeV. Global fits to large  $Q$  behavior, such as that discussed in the recent analysis of Ref. [45], find a small but still important contribution from the non-perturbative component of the evolution factor for values  $Q$  of order heavy vector boson masses. Another method for estimating the non-perturbative content of the  $b_T$ -dependence within the CSS formalism was given in Refs. [60, 66] and similarly finds that non-perturbative input remains important for  $Q$  of order heavy vector boson masses. Refs. [60, 66] further note that the relative contribution from the non-perturbative regime also has significant dependence on  $\sqrt{s}$ . By contrast, it has been suggested in Refs. [48–50], within the context of similar but alternative evolution formalisms, that accounting for non-perturbative evolution can be avoided entirely even at scales of order  $Q \sim 1.0$  to  $2.0$  GeV.

The question of the relevance of the non-perturbative region in the Collins TMD-factorization theorem may be addressed directly in the context of the COMPASS measurements by using the fits to estimate the important range of  $b_T$ .<sup>8</sup> We have plotted the fits obtained by the COMPASS collaboration [40] in coordinate space as the solid lines in Fig. 3. Since the transverse momentum space distribution is obtained from a two dimensional Fourier transform from the coordinate space expression, we have also included a factor of  $b_T$ . Also, since we are primarily interested in the width of the distribution, we normalize to unity in the integration over  $b_T$ . That is, instead of Eq. (23) the curves in Fig. 3 are for

$$\frac{b_T \langle P_T^2 \rangle}{2} \exp \left\{ -\frac{b_T^2 \langle P_T^2 \rangle}{4} \right\}. \quad (32)$$

Applying the integration  $\int_0^\infty db_T$  gives unity. Thus, up to a normalization, Eq. (32) is the integrand of the Fourier transform to coordinate space for the region of small  $P_T$ .

The initial and final Gaussian slope parameters  $\langle P_T^2 \rangle$  that we have used in Fig. 3 correspond to the *largest* parameter  $C_{\text{evol}}$  that is found in Tables I, II. This gives an estimate of the *maximum* reasonable rate of variation in the width with changes in  $Q$  of order  $\sim 1.0$  GeV and so is consistent with a strategy of placing rough upper limits on the rate of evolution that can reasonably be expected at low  $Q$ . The largest value for  $C_{\text{evol}}$  corresponds to the second row of the first entry in Table II, and the corresponding slope parameters from Ref. [40] are:

$$\langle P_T^2 \rangle_{Q_1=1.049 \text{ GeV}} = 0.1669 \pm 0.0012 \text{ GeV}^2; \quad \langle P_T^2 \rangle_{Q_2=2.114 \text{ GeV}} = 0.2325 \pm 0.0011 \text{ GeV}^2, \quad (33)$$

where the uncertainties are the quoted statistical uncertainties from the fit only.

The resulting curves shown in Fig. 3 are peaked around  $b_T \sim 3.0 \text{ GeV}^{-1}$  with tails extending out to nearly  $b_T \sim 10.0 \text{ GeV}^{-1}$ , i.e. up to transverse sizes about twice that of the proton charge radius, suggesting that the effect of non-perturbative input is substantial, at least in this region of moderate  $Q$ . For comparison, typical values for  $b_{\max}$  used in the CSS formalism are between about  $\sim 0.3 \text{ GeV}^{-1}$  [60] and  $\sim 1.0 \text{ GeV}^{-1}$  [44]. More relevant are estimates of the physical transverse distance scales over which non-perturbative physics is expected to become important. Using a chiral quark soliton model [29–32], Ref. [34] estimates a chiral symmetry breaking scale of about  $\sim 0.3 \text{ fm} \sim 1.5 \text{ GeV}^{-1}$  and a confinement scale of about  $5 \text{ GeV}^{-1}$ . These estimates are built on earlier instanton models [67–70] which likewise find a typical instanton size of  $\sim 0.3 \text{ fm}$ . The  $5 \text{ GeV}^{-1}$  confinement scale is also consistent with a proton charge radius of  $\sim 0.88 \text{ fm}$  [71] and a bag model radius of roughly  $\sim 1.2 \text{ fm}$  (See Ref. [72] and references therein).<sup>9</sup> Both

<sup>8</sup> Despite the notation, the  $b_T$  in the TMD-factorization formula is not an impact parameter like that appearing in generalized parton distributions for exclusive processes. Therefore, it should not be taken to represent the total size of either the target or final state hadron.

<sup>9</sup> We mention the bag model here since it continues to be used in non-perturbative model treatments of special TMD functions. See, for example, Refs. [73, 74].

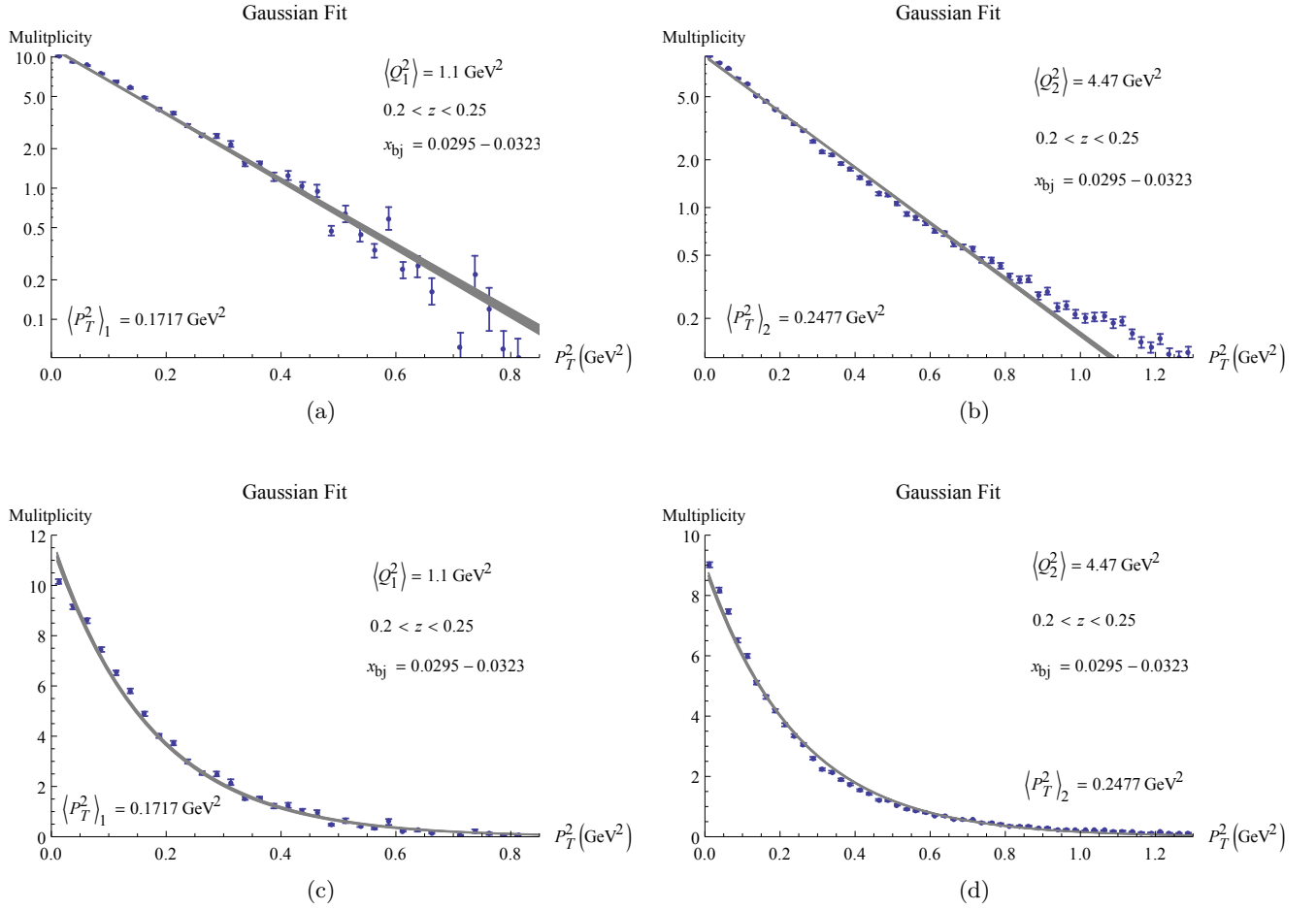


FIG. 4: (a) Gaussian fit for  $Q = 1.049 \text{ GeV}$ , all  $P_T$ . (b) Gaussian fit for  $Q = 2.114 \text{ GeV}$ , all  $P_T$ . (c, d) Same as (a, b) but on a linear axis. The gray band represents a 99% confidence band for the fit parameters, where only the reported statistical errors have been included. (See online for color.)

are of order  $1.0 \text{ fm} \sim 5.0 \text{ GeV}^{-1}$ . The points where various categories of non-perturbative physics are estimated to become relevant have been marked by arrows in Fig. 3.

From the general features of Fig. 3, we conclude that, for the differential cross section in the limit of  $P_T \rightarrow 0$ , the relevant range of  $b_T$  is likely to be nearly dominated by the non-perturbative region of  $b_T$  for  $Q \sim 1.0 \text{ GeV}$  to  $\sim 2.0 \text{ GeV}$ .

The robustness of this conclusion might be questioned on the grounds that the fits from [40] apply to a restricted range,  $P_T < 0.85 \text{ GeV}$ . One could speculate that including more of the large  $P_T$  tail might result in an enhanced relative contribution from small  $b_T$ . To address this, we have performed our own fit of the Gaussian form using the same data from Ref. [40] that gave the two curves for  $Q = 1.049 \text{ GeV}$  and  $Q = 2.114 \text{ GeV}$  in Fig. 3, but now for the entire range of  $P_T$  (up to  $P_T \gtrsim 1.0 \text{ GeV}$ ).<sup>10</sup> We perform the fitting in Wolfram Mathematica. The new Gaussian fits are shown in Fig. 4. From the plot, it is clear that the values we find for the Gaussian slopes,  $\langle P_T^2 \rangle_{Q_1=1.049 \text{ GeV}}$  and  $\langle P_T^2 \rangle_{Q_2=2.114 \text{ GeV}}$ , are so close to the COMPASS values that the curves in Fig. 3 are nearly unchanged, despite the inclusion of larger  $P_T$ . Instead of Eq. (33), we find:

$$\langle P_T^2 \rangle_{Q_1=1.049 \text{ GeV}}^{\text{New Fits}} = 0.1717 \pm 0.0011 \text{ GeV}^2; \quad \langle P_T^2 \rangle_{Q_2=2.114 \text{ GeV}}^{\text{New Fits}} = 0.2477 \pm 0.0008 \text{ GeV}^2, \quad (34)$$

<sup>10</sup> An accurate description of this large  $P_T$  region requires the  $Y$ -term rather than a fit based entirely on the TMD terms. However, fitting the TMD functions using the full range of  $P_T$  is a useful test of the sensitivity of our general conclusions about relevant ranges of  $b_T$  to the treatment of the  $P_T$  tail within fits.

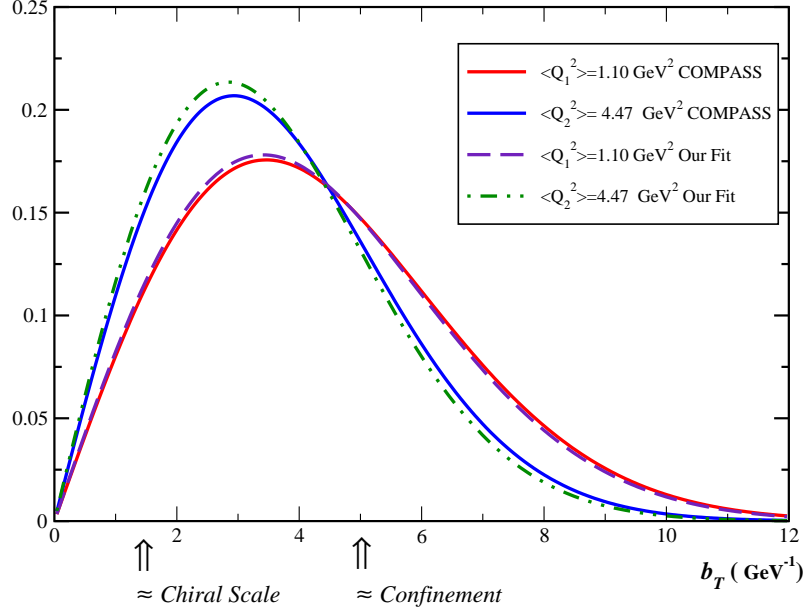


FIG. 5: Gaussian fits again showing the largest variation in the width found in Tables I, II. The solid red and blue curves are the same as those in Fig. 3, in which the fit is restricted to the region of  $P_T \leq 0.85$  GeV. The purple dashed and green dot-dashed curves are from the refit Gaussian curves in Fig. 4 that use all  $P_T$  and correspond to Eq. (32) with the initial and final  $\langle P_T^2 \rangle$  from Eq. (34). (See online for color.)

where again the uncertainties are statistical uncertainties from the fit only. The difference between the COMPASS fits in Eq. (33) and our fits in Eq. (34) for  $Q_1 = 1.049$  GeV is  $0.0048 \text{ GeV}^2$  and for  $Q_2 = 2.114$  GeV it is  $0.0152 \text{ GeV}^2$ . This difference gives a sense of the systematic uncertainty due to the upper cutoff on  $P_T$ . Note that this uncertainty is of order the values of  $C_{\text{evol}}$  found in Tables I, II and Fig. 2, suggesting that the precise value of  $C_{\text{evol}}$  has significant sensitivity to the way the large  $P_T$  region is cutoff.

To see how the new fits affect the coordinate space distribution, Eq. (32), we have replotted in Fig. 5 the original curves from Fig. 3 along with the curves using the new parameters in Eq. (34). It is clear that neglecting the large  $P_T$  values has little influence on the general features of the fits discussed above; namely, that there is a large contribution from intervals of  $b_T$  deep in the non-perturbative region.

A further critique could be made regarding the use of a Gaussian form on the grounds that analyticity considerations [34] imply a power law fall-off for the large  $P_T$  behavior of TMD correlation functions. Moreover, a power law behavior  $1/P_T^2$  (up to logarithmic corrections and the effects of evolution of collinear PDFs) is a prediction of pQCD (see, for example, Ref. [51]). This power law behavior is tied to singular behavior in the transverse position at small  $b_T$ .<sup>11</sup> Figure 4(b) shows that the Gaussian form does have some slight difficulty accounting for the full range of  $P_T$  for the larger  $Q_2 = 2.114$  GeV value. To address this, we have again refitted the  $Q_2 = 2.114$  GeV data but instead of Eq. (23), we have used a Kaplan functional form:

$$\frac{d\sigma}{dP_T^2} \propto \frac{1}{\left(1 + \frac{P_T^2}{M_{\text{kap}}^2}\right)^\nu}. \quad (35)$$

The result, shown in Fig. 6, gives a slightly more successful fit than the Gaussian fit of Fig. 4(b). When switching from the Gaussian fit to the Kaplan fit it is possible to quantify the goodness of the two fits. We use a straightforward

<sup>11</sup> The true large  $P_T$  behavior of the TMD functions is not directly meaningful at very large  $P_T$ , since TMD factorization (without the  $Y$  term) is inapplicable once the  $P_T$  is comparable with  $Q$ . Clearly, the  $Y$ -term will be need be incorporated in the future to deal with these issues.

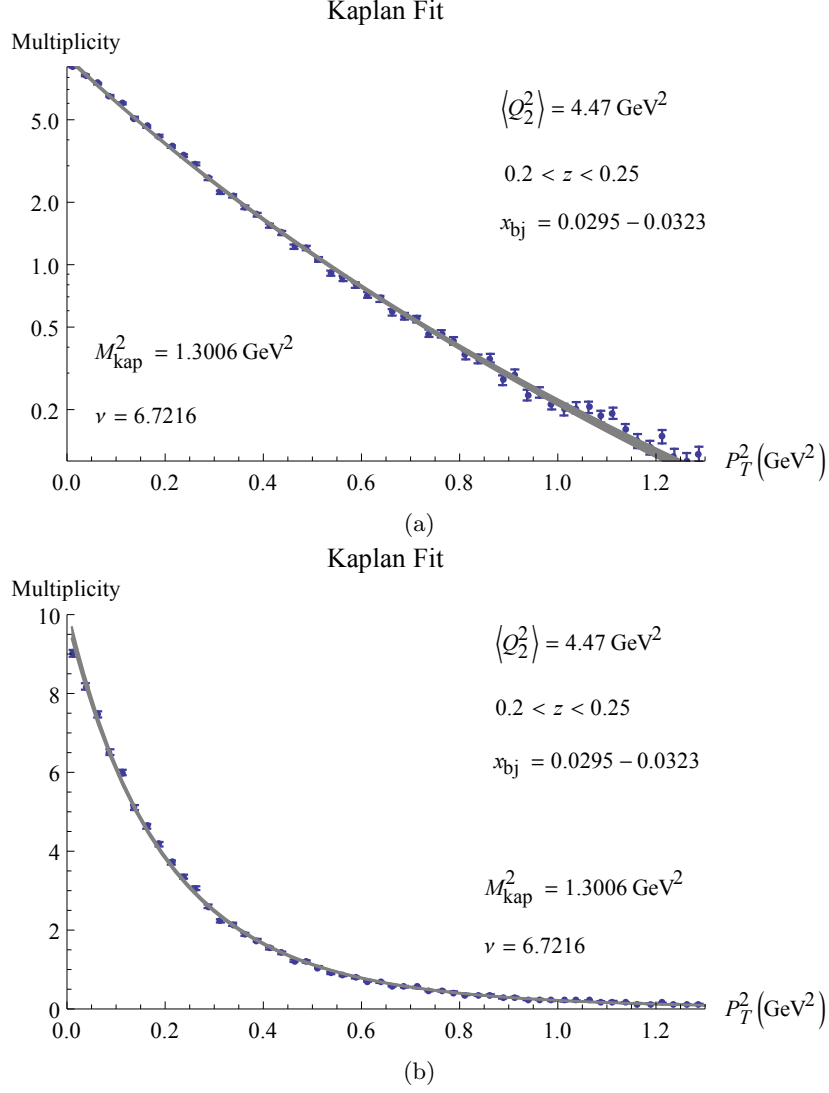


FIG. 6: Fits of the Kaplan function, Eq. (35), for  $Q = 2.114$  GeV and for all  $P_T$  with (a) a logarithmic plot and (b) a linear plot. The gray band represents a 99% confidence band for the fit parameters, where only the reported statistical errors have been included. (Color online.)

coefficient of determination,  $R^2$ , which is defined in the usual way [75] as  $1 - \text{SS}_{\text{res}}/\text{SS}_{\text{T}}$ , where  $\text{SS}_{\text{res}}$  is the residual sum of squares of each data point and the fit and  $\text{SS}_{\text{T}}$  is the total sum of squares. This coefficient is a simple measure of the goodness of the fit that approaches unity for a perfect fit. In this case, the  $R^2$  fit parameter rises modestly from 0.9918 to 0.9988 when moving from the Gaussian form to the Kaplan fit. The final Kaplan fit parameters are  $M_{\text{kap}}^2 = 1.3006 \text{ GeV}^2$  and  $\nu = 6.7216$ .

For the lower value of  $Q$ ,  $Q = 1.049$  GeV, the Gaussian form actually gives a better fit than the Kaplan form. Indeed, from Fig. 4(a) it can be seen that even the Gaussian fit tends to overshoot the data slightly at large  $P_T$ . This could be due to the role of resonances at very small  $Q$ .

As with the Gaussian form, we may examine the Kaplan fit in coordinate space. Instead of Eq. (32) we have

$$\frac{2b_T^\nu M_{\text{kap}}}{\Gamma(\nu)} \left( \frac{M_{\text{kap}}}{2} \right)^\nu K_{1-\nu}(b_T M_{\text{kap}}), \quad (36)$$

where  $K_{1-\nu}$  is the order  $1 - \nu$  modified Bessel function of the second kind. Again, we have imposed in Eq. (36) the normalization condition that the integration  $\int_0^\infty db_T$  is unity.

In coordinate space, the difference between the Gaussian and the Kaplan fits can be examined by comparing Eq. (36)

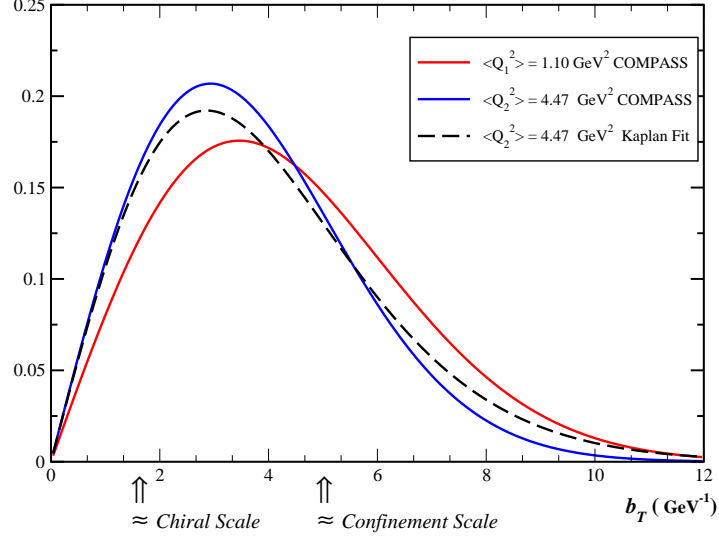


FIG. 7: The black dashed curve shows the  $b_T$  space function in Eq. (36) for  $Q_2 = 2.114$  GeV. This corresponds to the fit obtained in transverse momentum space using the Kaplan function in Eq. (35). The fits themselves are shown in Figs. 6 and yield parameters  $M_{\text{kap}}^2 = 1.3006$  GeV<sup>2</sup> and  $\nu = 6.7216$ . (See text for discussion.) For easy comparison, we have again included the solid red and blue curves from Fig. 3, corresponding to the original fits obtained by the COMPASS collaboration at  $\sqrt{\langle Q_1^2 \rangle} = 1.049$  GeV and  $\sqrt{\langle Q_2^2 \rangle} = 2.114$  GeV, respectively. (Color online.)

and Eq. (32) with the fit parameters corresponding to  $Q_2 = 2.114$  GeV. The result is shown in Fig. 7. Again, the original COMPASS fits from Fig. 3 are shown as the solid red ( $Q = 1.049$  GeV) and blue ( $Q_2 = 2.114$  GeV) curves. From Fig. 7, it can be seen that an analysis of the important regions of  $b_T$  leads to roughly the same conclusions as in the case of the Gaussian fit. We conclude that the general observation of this section – that regions of  $b_T$  deep into the non-perturbative regime are significant – is robust for  $P_T \rightarrow 0$  and for  $Q \sim 1$  GeV to  $\sim 2$  GeV, regardless of which functional form is used.

## VI. COMPARISON WITH TMD EVOLUTION

### A. Standard Evolution

Next, we examine the evolved formula in Eq. (21) to estimate how well it matches the change in widths of the Gaussian fits observed in Fig. 2 under different assumptions for  $g_K(b_T; b_{\text{max}})$ . Let us consider the coordinate space factor in Eq. (21) of the TMD term, including an overall factor of  $b_T$  in analogy with Eq. (32):

$$\frac{b_T}{N(Q)} \exp \left\{ -g_{\text{PDF}}(x, b_T; b_{\text{max}}) - g_{\text{FF}}(z, b_T; b_{\text{max}}) - 2g_K(b_T; b_{\text{max}}) \ln \left( \frac{Q}{Q_0} \right) + 2 \ln \left( \frac{Q}{\mu_b} \right) \tilde{K}(b_*; \mu_b) + \int_{\mu_b}^Q \frac{d\mu'}{\mu'} \left[ \gamma_{\text{PDF}}(\alpha_s(\mu'); 1) + \gamma_{\text{FF}}(\alpha_s(\mu'); 1) - 2 \ln \left( \frac{Q}{\mu'} \right) \gamma_K(\alpha_s(\mu')) \right] \right\}. \quad (37)$$

$N(Q)$  is defined to be the integral  $\int_0^\infty db_T$  of the numerator, so that the full quantity is normalized to unity when integrating over  $b_T$ . We will require that for  $Q = Q_0 = 1.049$  GeV, Eq. (37) reduces to the  $Q = 1.049$  GeV COMPASS

Gaussian fit shown in Fig. 3. That is, the input distributions are

$$\begin{aligned}
 & -g_{\text{PDF}}(x, b_T; b_{\text{max}}) - g_{\text{FF}}(z, b_T; b_{\text{max}}) \\
 & = -\frac{b_T^2 \langle P_T^2 \rangle_{Q_0}}{4} - 2 \ln \left( \frac{Q_0}{\mu_b} \right) \tilde{K}(b_*; \mu_b) - \int_{\mu_b}^{Q_0} \frac{d\mu'}{\mu'} \left[ \gamma_{\text{PDF}}(\alpha_s(\mu'); 1) + \gamma_{\text{FF}}(\alpha_s(\mu'); 1) - 2 \ln \left( \frac{Q_0}{\mu'} \right) \gamma_K(\alpha_s(\mu')) \right].
 \end{aligned} \tag{38}$$

With this choice for  $-g_{\text{PDF}}(x, b_T; b_{\text{max}}) - g_{\text{FF}}(z, b_T; b_{\text{max}})$ , Eq. (37) reduces exactly to Eq. (32) at  $Q = Q_0$ .<sup>12</sup>

We use the one-loop  $\overline{\text{MS}}$  expressions for the anomalous dimensions with  $C_1 = 2e^{-\gamma_E}$ , which are included in App. A for reference. We use the approximation  $\alpha_s(\mu) = 1/2\beta_0 \ln(\mu/\Lambda_{\text{QCD}})$  for the running coupling with 3 flavors and  $\Lambda_{\text{QCD}} = 0.2123 \text{ GeV}$ . (See App. B for more discussion of  $\alpha_s(\mu)$  and the choice of  $\Lambda_{\text{QCD}}$ .) Then, the integrals in the one loop anomalous dimensions may be straightforwardly evaluated to obtain analytic expressions for all perturbative parts of the exponent in Eq. (37). The explicit expression is given in App. C.

For  $g_K(b_T; b_{\text{max}})$ , we start by using Eq. (22), with a conservative  $b_{\text{max}} = 0.5 \text{ GeV}^{-1}$  and several sample values of  $g_2(b_{\text{max}})$ . We compare with the maximum observed rate of evolution seen in the COMPASS data – the curves already shown in Fig. 3. The results are shown in Fig. 8(a) and (c), where the dot-dashed curves show the evolution to  $Q^2 = 4.47 \text{ GeV}^2$  for a range of sample values for  $g_2$ . There is ambiguity as to which values of  $Q_0$  and  $Q$  should be used in the evolution, given the differences between  $Q^{\text{min}}$ ,  $Q^{\text{max}}$  and  $\sqrt{\langle Q^2 \rangle}$  in Tables I, II. In order to estimate roughly the approximate size of evolution effects, we will continue to use  $\sqrt{\langle Q^2 \rangle}$  for the the initial and final values of  $Q$ .

We begin with  $g_2 = 0$  and see essentially no effect on the  $b_T$  distribution when  $Q$  is varied; the integrand is small in the region of small  $b_T$  where perturbative evolution would be substantial, and setting  $g_2 = 0$  suppresses any non-perturbative contribution to evolution. Next, we consider  $g_2 = C_{\text{evol}}$ , with the maximum value of  $C_{\text{evol}} = 0.0306 \text{ GeV}^2$  found in Tables I, II. Finally, we consider  $g_2 = 0.1 \text{ GeV}^2$  and  $g_2 = 0.7 \text{ GeV}^2$  which are values more typical of fits obtained at large  $Q$ , as well as the renormalon analysis value of  $g_2 = 0.19 \text{ GeV}^2$  in Ref. [54]. (See, also, Fig. 1 of Ref. [44].)

We have repeated this exercise for the much more liberal value of  $b_{\text{max}} = 2.0 \text{ GeV}^{-1}$ , and the result is shown in Figs. 8 (b) and (d). In Figs. 8(a)-(d), a value of  $g_2(b_{\text{max}}) \lesssim C_{\text{evol}}^{\text{max}}$  is clearly preferred over values of  $g_2(b_{\text{max}}) \geq 0.1 \text{ GeV}^2$ . Note that with  $g_2 = 0$ , there is very weak evolution in the  $b_T$  shape relative to the variations in the width suggested by the COMPASS data in the small range of  $Q$  values. A choice of  $g_2 = C_{\text{evol}}^{\text{max}} = 0.0306 \text{ GeV}^2$  is roughly consistent with the upper limit on the rate of evolution observed in Tables I, II and Fig. 2. Thus, if we demand the ansatz in Eq. (22) for the form of  $g_K(b_T; b_{\text{max}})$  for all  $b_T$ , then we estimate that the true value of  $g_2$ , at least for the kinematics of Tables I, II, must lie roughly in the range of  $0 < g_2 \lesssim 0.03 \text{ GeV}^2$ .

## B. Modified Large $b_T$ Behavior

Because of the strong universality of  $g_K(b_T; b_{\text{max}})$ , the results of the last section seem on the surface to indicate a discrepancy between the low  $Q$  data and detailed and successful fits of the past that focus on larger  $Q$ , which tend to find  $g_2 \gtrsim 0.1 \text{ GeV}^2$  [15, 16, 43, 44]. For instance, values of  $g_2$  have been found to be as large as  $0.68 \text{ GeV}^2$  [43], and a value of  $g_2 = 0.19 \text{ GeV}^2$  is used in Ref. [16] for SIDIS in the CSS formalism, both using a value of  $b_{\text{max}} = 0.5 \text{ GeV}^{-1}$ . Moreover, the renormalon analysis of Ref. [54] also suggests a  $g_2$  of similar size for small  $b_T$ . (See, also, Fig. 1 of Ref. [44].) However, the quadratic ansatz in Eq. (22) (which gives a Gaussian ansatz when it appears in the exponent of Eq. (21)) seems to impose excessive suppression of the very large non-perturbative  $b_T$  region whenever  $g_2 \gtrsim 0.1 \text{ GeV}^2$ . A critique of the purely Gaussian non-perturbative form was also given in Ref. [60], where it was argued that the Gaussian form gives excessive sensitivity to non-perturbative input at large transverse momentum, and a power law,  $\sim b_T^{0.3}$ , with a  $b_{\text{max}} = 0.3 \text{ GeV}^{-1}$  is suggested, though this is possibly an overly conservative choice, given our earlier discussion of  $b_T$  regions in Fig. 3, and given that scales  $\geq 3.0 \text{ GeV}$  are generally considered to be well within the perturbative region. See related discussions of this in Ref. [44].

To resolve the apparent discrepancy discussed above, we recall that large  $Q$  fits, e.g. for  $Q \gtrsim 10 \text{ GeV}$ , are sensitive mainly to the region of  $b_T \lesssim 2.0 \text{ GeV}^{-1}$ . See, for example, Fig. 4 of Ref. [44] and compare this with Fig. 3, where contributions from  $b_T \gtrsim 2.0 \text{ GeV}^{-1}$  dominate. Now let us assume that non-perturbative effects become totally

<sup>12</sup> Recall, however, the note of caution immediately following Eq. (25).



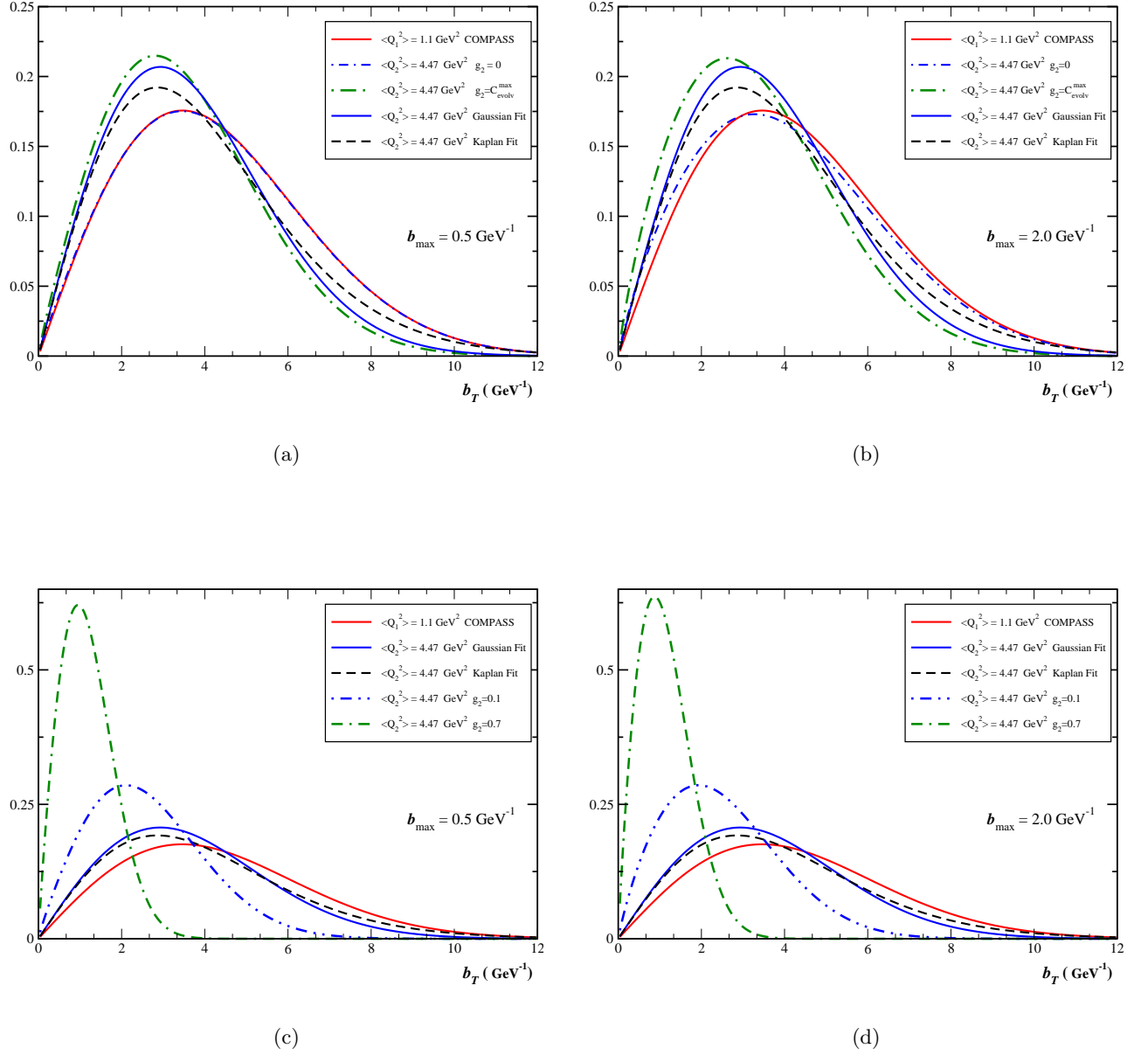


FIG. 8: Left Panels (a) and (c): The solid red and blue lines (see online for color) are the same initial and final Gaussian fits obtained by COMPASS as in Fig. 3 for  $Q_1^2 = 1.1 \text{ GeV}^2$  and  $Q_2^2 = 4.47 \text{ GeV}^2$  respectively. The black dashed curve is the Kaplan fit for  $Q^2 = 4.47 \text{ GeV}^2$ , already shown in Fig. 7. The dot-dashed lines are the TMD factorization expression in Eq. (37) for the evolution to  $Q_2^2 = 4.47 \text{ GeV}^2$  with the Gaussian ansatz from Eq. (22) for  $g_K(b_T; b_{\text{max}})$  with  $b_{\text{max}} = 0.5 \text{ GeV}^{-1}$ . The positions of the peaks of the evolved distributions decrease with increasing  $g_2$ : Figure (a) shows the results for  $g_2 = 0$  (blue dot-dashed) and  $C_{\text{evol}}^{\text{max}} = 0.0306 \text{ GeV}^2$  (green dot-dashed); Figure (c) shows the result for  $g_2 = 0.1 \text{ GeV}^2$  (blue dot-dashed) and  $g_2 = 0.7 \text{ GeV}^2$  (green dot-dashed). All curves are normalized to one in the integration over  $b_T$ . Right Panels (b) and (d): Same as the left panels, but for  $b_{\text{max}} = 2.0 \text{ GeV}^{-1}$ .

dominant at some large size scale  $b_{\text{NP}}$ , where  $g_K(b_T; b_{\text{max}})$  acquires a more complicated and as-yet unknown precise form. Recall also that  $g_K(b_T; b_{\text{max}})$  is predicted to vanish as a power of  $b_T^2$  at small  $b_T$  [53–56]. Thus, for  $b_T \ll b_{\text{NP}}$  the following expansion applies:

$$g_K(b_T; b_{\text{max}}) = a_1 \left( \frac{b_T^2}{b_{\text{NP}}^2} \right) + a_2 \left( \frac{b_T^4}{b_{\text{NP}}^4} \right) + \dots \quad (39)$$

See also Eq. (6.1) of Ref. [54].<sup>13</sup> We conjecture that large  $Q$  fits typically obtain a large  $g_2$  because they are sensitive only to the first power-law correction in Eq. (39). By contrast, at smaller  $Q$  higher powers, and eventually the complete functional form, become important.

We propose that the optimal way to proceed is to use a functional form for  $g_K(b_T; b_{\text{max}})$  that: a.) respects its strong universality set forth in TMD factorization by matching to earlier large  $Q$  fits that use a Gaussian form but b.) avoids strong disagreement with the results of the empirical analysis of SIDIS data from Sect. V. Thus, we impose the following conditions:

- At small  $b_T^2$ , the lowest order coefficient in Eq. (39), i.e.  $a_1/b_{\text{NP}}^2$ , must be roughly  $\gtrsim 0.1 \text{ GeV}^2$  in order to be consistent with the values of  $g_2/2$  found in Ref. [15, 16, 43, 44, 54], thereby respecting the strong universality of  $g_K(b_T; b_{\text{max}})$ .
- At  $b_T \gg b_{\text{NP}}$ ,  $g_K(b_T; b_{\text{max}})$  should become nearly constant, or at most logarithmic in  $b_T$ .

As a simple example, we propose

$$g_K(b_T; b_{\text{max}}) = \frac{g_2(b_{\text{max}})b_{\text{NP}}^2}{2} \ln \left( 1 + \frac{b_T^2}{b_{\text{NP}}^2} \right). \quad (40)$$

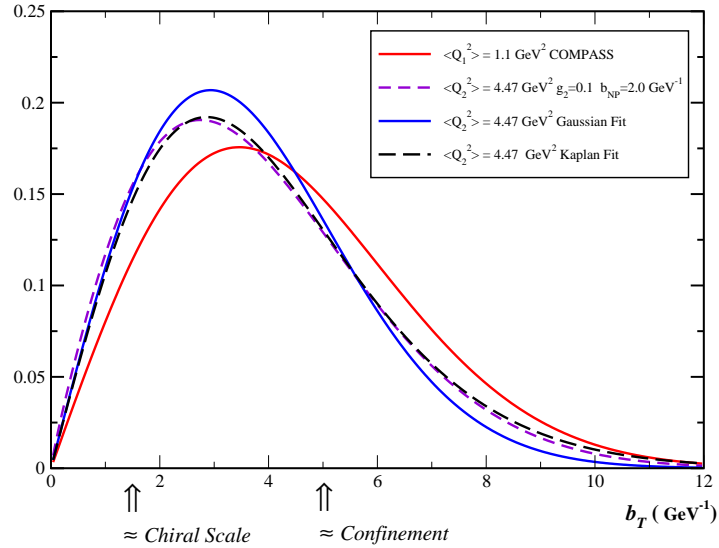


FIG. 9: The solid red and blue curves are again the same initial and final Gaussian fits obtained by COMPASS for  $Q^2 = 1.1 \text{ GeV}^2$  and  $Q^2 = 4.47 \text{ GeV}^2$  respectively – the same as in Fig. 3. (See online for color.) The black dashed curve is again the Kaplan fit for  $Q^2 = 4.47 \text{ GeV}^2$  already shown in Fig. 7. For comparison, the purple short-dashed curve is the TMD factorization expression in Eq. (37), but now using Eq. (40) for  $g_K(b_T; b_{\text{max}} = 0.5 \text{ GeV}^{-1})$  with  $b_{\text{NP}} = 2.0 \text{ GeV}^{-1}$  and  $g_2 = 0.1 \text{ GeV}^2$ . This should be compared with the  $g_2 \geq 0.1 \text{ GeV}^2$  curves in Fig. 8 where the quadratic ansatz for  $g_K(b_T; b_{\text{max}})$  – Eq. (22) – is used.

<sup>13</sup> Note, however, that Ref. [54] predicts a linear rather than constant dependence at very large  $b_T$ .

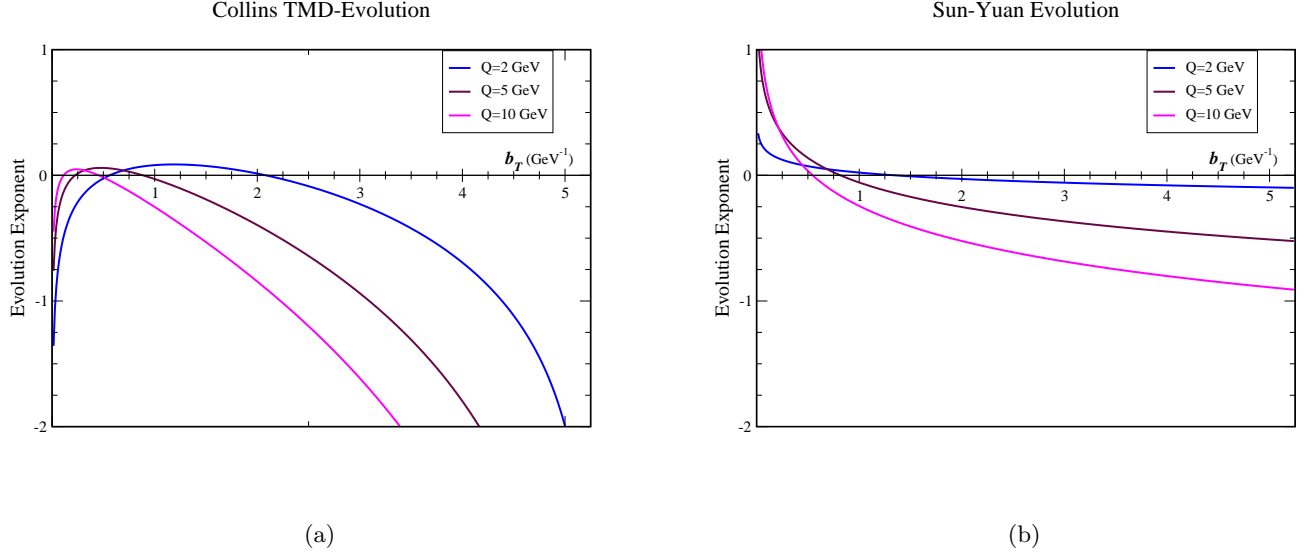


FIG. 10: The  $Q$  dependent terms in the perturbative parts of the exponents in (a) Eq. (37) for the TMD factorization formalism and (b) Eq. (42) for the Sun-Yuan formalism.

(See, also, Eq. (6.14) of Ref. [54].) Expanding around  $b_T \ll b_{\text{NP}}$  gives the first two terms,

$$g_2(b_{\text{max}}) \frac{1}{2} b_T^2 - g_2(b_{\text{max}}) \frac{1}{4b_{\text{NP}}^2} b_T^4 + \dots \quad (41)$$

In Fig. 9 we illustrate how the low  $Q$  dependence of the COMPASS data may be accommodated into earlier larger  $Q$  fits by using the modified  $g_K(b_T; b_{\text{max}})$  from Eq. (40) with  $b_{\text{max}} = 0.5 \text{ GeV}^{-1}$ ,  $g_2 = 0.1 \text{ GeV}^2$  and  $b_{\text{NP}} = 2.0 \text{ GeV}^{-1}$ .<sup>14</sup> Since the lowest order term in the expansion in Eq. (41) matches Eq. (22) with  $g_2 = \mathcal{O}(0.1 \text{ GeV}^2)$  and thus is generally consistent with earlier fits such as Ref. [15, 16]. In this way, moderate  $Q$  data may be accommodated without introducing disagreement with important and universal non-perturbative contributions obtained in earlier fits, while simultaneously giving access to further universal non-perturbative information.

For now we propose Eq. (40) only as a simple example of how  $g_K(b_T; b_{\text{max}})$  might possibly be modified at very large  $b_T$ . In practice, better and more detailed parametrizations may be needed, possibly obtainable from non-perturbative studies.

## VII. COMPARISON BETWEEN COLLINS AND SUN-YUAN FORMALISM

In Ref. [49, 50], Sun and Yuan argue that an alternative evolution factor should be adopted for the region of  $Q \lesssim 10 \text{ GeV}$ . In their approach, the TMD PDFs are evolved relative to an arbitrary scale  $Q_0 \sim 1.0 \text{ GeV}$  rather than the intrinsic hard scale  $\sim 1/b_T$  of the TMD PDF. Thus the Sun-Yuan formalism contains unresummed logarithms of  $b_T$ . The Sun-Yuan form of evolution replaces the exponential factor in Eq. (37) with,

$$b_T \exp \left\{ -\frac{b_T^2 \langle P_T^2 \rangle_0}{4} \right\} \exp \left\{ -2C_F \int_{Q_0}^Q \frac{d\mu'}{\mu'} \frac{\alpha_s(\mu')}{\pi} \left[ \ln \left( \frac{Q^2}{\mu'^2} \right) + \ln \left( \frac{Q_0^2 b_T^2}{C_1^2} \right) - \frac{3}{2} \right] \right\}. \quad (42)$$

See Eq. (3) of Ref. [49] and Eq. (77) of Ref. [50]. It is arrived at by extending a low order calculation of the  $b_T$ -dependence into the region of very large  $b_T$ . From the point of view of doing practical calculations, there appears to be an advantage in that there is no explicit Landau pole encountered in the evaluation of  $\alpha_s(\mu)$  and thus, on the surface, no need to include a non-perturbative component to the evolution. (See the discussion immediately before and after Eq. (3) in Ref. [49] for the rationale and motivation given to use this form rather than the Collins TMD factorization or

<sup>14</sup> In general,  $b_{\text{NP}}$  may also be a function of  $b_{\text{max}}$  but to simplify notation we do not show it explicitly in Eq. (40).

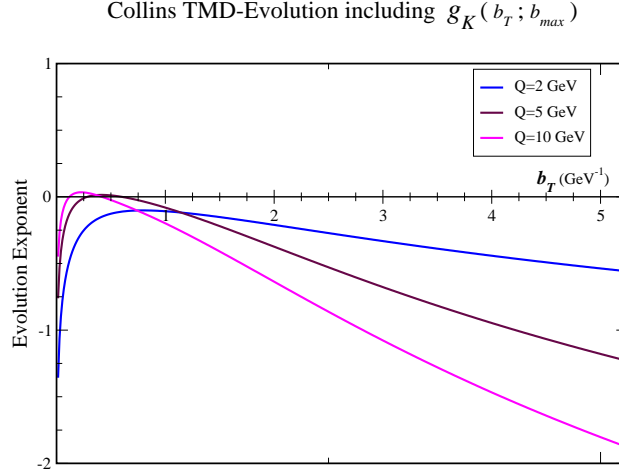


FIG. 11: The  $Q$  dependent terms in the Collins TMD factorization formalism exponents from Eq. (37) using the large- $b_T$  function  $g_K(b_T; b_{\max})$  in the form of Eq. (40) with  $g_2 = 0.1 \text{ GeV}^2$ ,  $b_{\text{NP}} = 2.0 \text{ GeV}^{-1}$  and with  $b_{\max} = 0.5 \text{ GeV}^{-1}$ .

CSS form.) By contrast, in the Collins TMD-factorization approach, the region of smaller  $Q$  is where the genuine non-perturbative  $b_T$ -dependence is understood to become increasingly important, including in the evolution. The Collins TMD-factorization formalism includes a strategy of isolating and testing the strong universality of non-perturbative behavior at large  $b_T$  while matching to an optimal perturbative treatment at  $b_T \ll 1/\Lambda_{\text{QCD}}$ . Both the standard CSS formalism and the Collins TMD factorization formalism predict a greater input from non-perturbative evolution over low regions of  $Q$ . Conversely, Sun-Yuan argue that the non-perturbative component is needed for evolution at large  $Q$  but is negligible in the vicinity of small  $Q$ .

While it is beyond the scope of this article to make a full comparison between these two approaches (see, however, Ref. [76]), it is worthwhile to examine briefly whether the two formalisms are essentially equivalent ways of implementing the same evolution or whether they are in contradiction with one another. To this end, we note that the purely perturbative contributions give rather different evolution exponents in the region of  $Q \lesssim 10 \text{ GeV}$ . This can be seen by directly computing the exponents in both Eq. (37) and Eq. (42) using the one-loop expressions for the anomalous dimensions and the running coupling. The resulting analytic expressions for both the Collins TMD-factorization case and the Sun-Yuan case are given in App. C. In Fig. 10(a) we have plotted the exponent of the evolution factor in Eq. (37), keeping only the perturbative parts and dropping the  $g_K(b_T; b_{\max})$ . We have set  $b_{\max}$  to infinity so that it is a purely perturbative expression with no explicit cutoff functions like Eq. (13). In Fig. 10(b) we have plotted, for comparison, the Refs. [49, 50] evolution exponent from Eq. (42). For  $Q_0$  we use  $Q_0 = \sqrt{2.4} \text{ GeV}$  which is the value used in Refs. [49, 50]. As in this article, Refs. [49, 50] neglect the  $Y$  term and only account for the role of the TMD term.

Even in the region of  $1.0 \text{ GeV} \lesssim Q \lesssim 10.0 \text{ GeV}$ , it can be seen from these graphs that there are significant differences, both qualitatively and quantitatively, between the Collins and Sun-Yuan treatment of the perturbative parts of the evolution exponents. In addition, it is worth noting that Eq. (42) does not obey Eq. (27) for the TMD term, as can be checked explicitly using Eq. (C2). The main difference is in the region of very small  $b_T$  where the two expressions diverge with opposite signs. In the Collins TMD factorization treatment,  $\alpha_s$  is allowed to run with  $\sim 1/b_T$  in both the CS kernel and in the TMD functions in such a way as to optimize the perturbative treatment in the small regions of  $b_T$ , whereas in the Sun-Yuan case the evolution is relative to a fixed scale  $\mu_0$ . As is clearly acknowledged in Refs. [49, 50], the Sun-Yuan treatment of evolution must break down at large  $Q$  (in fact it diverges above some  $Q$ ) as the integrand of the Fourier transform becomes increasingly concentrated around perturbatively small  $b_T$ . In the Collins TMD factorization treatment, the evolution involves true non-perturbative physics at large  $b_T$  whereas the Sun-Yuan formalism retains a perturbative treatment at large  $b_T$ . Thus, the treatments differ at both large and small  $b_T$ .

It is worth further investigating the origin of the difference between Fig. 10(a) and (b). Because  $\alpha_s$  does not run with  $\sim 1/b_T$  in the Sun-Yuan kernel, it has very weak  $b_T$ -dependence in the region of very large  $b_T$ , so that on the surface there does not appear to be the same sensitivity to non-perturbative large  $b_T$  physics as in the Collins

TMD factorization treatment. However, our analysis from Sect. V suggests that much of the relevant  $b_T$  range in Figs. 10(a,b) is well into the region characterized by the type of genuine non-perturbative physics one hopes to extract in a TMD analysis.

Taking into account the details of the non-perturbative part of the large  $b_T$  behavior, such as is described in Sect. VI B, allows one to obtain a reasonable description of the large  $b_T$  behavior in a way that agrees with the qualitative behavior of the COMPASS data while still matching to the optimized perturbative TMD factorization form of evolution from Ref. [3] in the limit of small  $b_T < b_{\max}$ . Thus the Collins TMD-factorization formalism unifies the large and small  $Q$  behavior in a single evolution formalism. To illustrate this, we have replotted Fig. 10(a) in Fig. 11, but now with the  $g_K(b_T; b_{\max})$  term included and using the sample functional form in Eq. (40) with  $b_{\max} = 0.5 \text{ GeV}^{-1}$ ,  $g_2 = 0.1 \text{ GeV}^2$ , and  $b_{\text{NP}} = 2.0 \text{ GeV}^{-1}$ .

Also, compare the categorization of relevant regions of  $b_T$  at  $Q \sim 2.0 \text{ GeV}$  in Figs. 3, 5, and 7 with Figs. 10 and 11. From this we can see that the main difference between the Collins and Sun-Yuan treatments at  $Q$  of  $\sim 1.0 \text{ GeV}$  to  $2.0 \text{ GeV}$  is in how non-perturbative, large size regions of  $b_T$  behavior are taken into account. The reliably perturbative, small  $b_T$ -behavior gives only a rather small contribution for such kinematics.

As  $Q$  increases above  $\sim 2.0 \text{ GeV}$ , sensitivity to the treatment of perturbation theory at small  $b_T$  becomes increasingly important. Future improvements to the global implementation of evolution, combined with increasingly sensitive experiments, may possibly be able to distinguish between the two ways of dealing with the perturbative component of evolution at small  $b_T$  in future data even in the range of  $Q \sim 2.0 \text{ GeV}$  to  $10.0 \text{ GeV}$ .

## VIII. DISCUSSION

Since evolution gives the variation with respect to  $Q$  (with all other variables fixed) then in principle a much larger range of  $Q$  values than in Tables I, II needs to be taken into consideration in order to obtain reasonable constraints on the non-perturbative input to  $g_K(b_T; b_{\max})$ . We stress, therefore, that what we have presented in this paper should not be regarded as a self-contained fitting project, but rather an investigation of general features of moderate  $Q$  behavior that need to be accounted for in treatments that operate within a complete TMD factorization formalism and with the goals and strategies outlined in the introduction. Even with the small variations in  $Q$  discussed in this paper, however, one is able to constrain general properties of  $g_K(b_T; b_{\max})$ . That the data are at relatively low  $Q$  helps especially to constrain the form of the non-perturbative evolution function  $g_K(b_T; b_{\max})$  in regions of very large  $b_T$  that are inaccessible in fits that focus on large  $Q$ . Our method of extracting of the weak  $Q$  dependence considers variations in  $Q$  within a single experiment at fixed  $x$  and  $z$  bins. To analyze several bins in  $Q^2$ , and thus place meaningful constraints on evolution, we considered smaller  $x$  values, relative to the valence region, in Tables I, II and Figs. 2 (a) and (b).

Our analysis is framed within the context of the Collins TMD factorization theorem, and by allowing a more general treatment of the non-perturbative component of the CS kernel than the usual power law, we find that we may extend TMD factorization to lower  $Q$  SIDIS measurements with no need to distort the perturbative part of evolution that is necessary to unify low  $Q$  cross section measurements with large  $Q$  ones. Moreover, we are able to maintain consistency with prior successful fits of non-perturbative parts done at larger  $Q$ . Finally, by maintaining the basic framework of Ref. [3] we are able to focus on what can be learned about the non-perturbative yet totally universal component of evolution, thereby accessing fundamental non-perturbative information.

Figures 2 (a) and (b) demonstrate that, although the variation in the  $P_T$ -shape with  $Q$  is small, there is evidence of non-zero broadening due to Collins-Soper evolution. The size of the evolution can be estimated from the range of values for  $C_{\text{evol}}$  found in Tables I, II.

Tables I, II and Figs. 2 (a) and (b) show some variation of  $C_{\text{evol}}$  with  $x$  and  $z$ . Also, comparing Tables I, II, one sees a trend of larger  $C_{\text{evol}}$  for the production of negative hadrons than for positive hadrons. This suggests that a description in terms of the TMD term alone is a poor approximation at these relatively low values of  $Q$ , and that the  $Y$ -term is in certainly needed. Details of the calculation of the entries in Tables I, II and of our plots will be made available at [64].

In addition to the recalling the important role of the  $Y$ -term, some other words of caution are necessary. A possible limitation of TMD studies such as this one, done at such small  $Q$ , is that they may begin to approach the boundary of the region of applicability for the TMD factorization formalism. The TMD factorization theorem describes the transversely differential cross section in terms of three distinct kinematical regions: The lowest transverse momenta are of order  $\lesssim \Lambda_{\text{QCD}}$ , and transverse momentum dependence is understood here to be intrinsic and non-perturbative. The second relevant region is where transverse momenta are large, of order  $P_T \sim Q$ , where transverse momentum dependence is described purely in terms of higher order collinear factorization (i.e., in terms of the  $Y$ -term alone). Finally there is an intermediate third region where  $\Lambda_{\text{QCD}} \ll P_T \ll Q$ . Here, the TMD-factorization description applies, but the TMD PDFs are expressible in terms of collinear parton distributions. A reliable description of the

cross section in this last region requires both the TMD term and the  $Y$ -term to be present. Note that the derivation of the TMD factorization theorem requires the use of approximations specific to each region separately.

In the region approaching  $Q \sim 1.0$  GeV, the distinction between the different regions of  $P_T$  becomes less clear. For instance, while the region of  $P_T \sim 0.5$  GeV is generally expected to have a significant non-perturbative contribution, it is not clear that the approximation  $P_T \ll Q$  is then reasonable for  $Q$  of only 1.0 GeV. Moreover, hadronic mass effects may become important when  $Q$  is of order only a few GeV. Thus, it may be that the kinematics of the process need to be treated more exactly in an extended formalism, such as in the formalism proposed in Ref. [77]. Finally, we recall again that flavor dependence will likely play an important role, as emphasized recently in Ref. [37].

However, the general trends that we observe are dramatic enough that we expect our main conclusions to be robust. Even considering the issues related to the  $Y$ -term and possible limitations of TMD-factorization at very low  $Q$  discussed above, it is difficult to reconcile the small values of  $C_{\text{evol}}$  found in Tables I, II with the much larger non-perturbative soft evolution found from direct extrapolations of global fits of Drell-Yan or large  $Q$  processes to much lower  $Q$ , if one limits the treatment of the non-perturbative large  $b_T$  evolution factor to the quadratic form in Eq. (22) for all  $b_T$ . In this regard, we confirm one of the main observations of Ref. [49, 50].

However, the meaning that we extract from these observations is rather different from Ref. [49, 50]. In our analysis, performed within the TMD factorization theorem of Ref. [3], we find much greater sensitivity to the details of the non-perturbative large  $b_T$  structure, rather than evidence that non-perturbative contributions to evolution are unnecessary. Moreover, we find that the complications that arise from extrapolating from large  $Q$  arise because of the greater care necessary in treating the non-perturbative contribution to evolution as larger  $b_T$  values becomes relevant. The lack of such a detailed account is a limitation of the TMD parametrizations produced in Ref. [58]. By accounting for the non-perturbative behavior at very large  $b_T$ , as discussed in Sect. VIB, we find that it is not difficult to reconcile past large  $Q$  fits of non-perturbative evolution with the moderate  $Q$  fits; see Fig. 9. Finally, our treatment of the perturbatively calculable parts of the evolution differs from that of Ref. [49, 50], as discussed in Sect. VII.

In future fits, more detailed treatments of the functional form for  $g_K(b_T; b_{\text{max}})$  at large  $b_T$  will be important both for extending TMD factorization to lower  $Q$  where studies in hadronic structure are often performed, and for achieving the increasing demands for high precision at large  $Q$ . Reliable constraints on  $g_K(b_T; b_{\text{max}})$  might be obtained from global fitting that includes the  $Y$ -term and proper matching to collinear factorization at small  $b_T$ , such as is done in Refs. [15, 16], but including newer low  $Q$  data and alternative functional forms for  $g_K(b_T; b_{\text{max}})$ . Another possibility is to repeat global fits to Drell-Yan type processes, but with the species of colliding hadrons held fixed. (See, also, the recent review of novel Drell-Yan phenomenology in Ref. [78].) An important achievement would be to successfully identify differences in the transverse momentum dependence between different types of colliding hadrons, i.e. between valence and sea quark distributions, as discussed in the introduction. Addressing this and similar issues within a complete TMD factorization formalism will help to unify TMD evolution studies with hadronic structure phenomenology while also addressing fundamental non-perturbative issues like those raised in Ref. [34, 35].

## Appendix A: TMD PDF $\overline{\text{MS}}$ Anomalous Dimensions

The anomalous dimensions to order  $\alpha_s(\mu)$  are the same for the TMD PDF and the TMD fragmentation function:

$$\gamma_{\text{PDF}}(\alpha_s(\mu), \zeta_{\text{PDF}}/\mu^2) = 4C_F \left( \frac{3}{2} - \ln \left( \frac{\zeta_{\text{PDF}}}{\mu^2} \right) \right) \left( \frac{\alpha_s(\mu)}{4\pi} \right) + \mathcal{O}(\alpha_s(\mu)^2), \quad (\text{A1})$$

$$\gamma_{\text{FF}}(\alpha_s(\mu), \zeta_{\text{FF}}/\mu^2) = 4C_F \left( \frac{3}{2} - \ln \left( \frac{\zeta_{\text{FF}}}{\mu^2} \right) \right) \left( \frac{\alpha_s(\mu)}{4\pi} \right) + \mathcal{O}(\alpha_s(\mu)^2). \quad (\text{A2})$$

The  $\overline{\text{MS}}$  anomalous dimension of the CS kernel to one loop is

$$\gamma_K(\alpha_s(\mu)) = 8C_F \left( \frac{\alpha_s(\mu)}{4\pi} \right) + \mathcal{O}(\alpha_s(\mu)^2). \quad (\text{A3})$$

$C_F = 4/3$  for QCD.

## Appendix B: Running Coupling

For running coupling, we use the form

$$\alpha_s(\mu) = \frac{A}{2 \ln(\mu/\Lambda_{\text{QCD}})}, \quad (\text{B1})$$

which will allow us to easily obtain low order analytic expressions for perturbative quantities. Here,

$$A = \frac{1}{\beta_0} = \frac{12\pi}{33 - 2n_f} = \frac{9}{4\pi}. \quad (\text{B2})$$

Since we are interested in the behavior in the neighborhood of  $\mu \sim 1.0$  GeV, we use  $n_f = 3$ . To determine a value for  $\Lambda_{QCD}$ , we fit to the three loop  $\beta$  function 2009 world average for  $\alpha_s(\mu)$  in Ref. [79] in the region of 1.1 GeV to 3 GeV. We find  $\Lambda_{QCD} = 0.2123$  GeV. Equation B1 then closely matches the three loop behavior in the region of  $\sim 1.0$  GeV, though the three loop  $\beta$  function rises more steeply at small  $\mu$ . Thus, our calculations are consistent with a slight underestimate of the approach to the non-perturbative region.

### Appendix C: Evolution Exponents To One Loop

Using Eq. (B1) and Eqs. (A1)-(A3) inside Eq. (37), we may calculate the perturbative part of the evolution factor in the Collins TMD factorization formalism analytically. The result is,

$$\begin{aligned} & \int_{\mu_b}^Q \frac{d\mu'}{\mu'} \left[ \gamma_{\text{PDF}}(g(\mu'); 1) + \gamma_{\text{FF}}(g(\mu'); 1) - 2 \ln \left( \frac{Q}{\mu'} \right) \gamma_K(g(\mu')) \right] \\ &= \frac{2A}{\pi} \left[ \ln \left( \frac{\ln(Q/\Lambda_{QCD})}{\ln(\mu_b/\Lambda_{QCD})} \right) - \frac{4}{3} \ln(Q/\Lambda_{QCD}) \ln \left( \frac{\ln(Q/\Lambda_{QCD})}{\ln(\mu_b/\Lambda_{QCD})} \right) + \frac{4}{3} \ln(Q/\mu_b) \right]. \end{aligned} \quad (\text{C1})$$

Note that we have dropped the  $\tilde{K}(b_*; \mu_b)$  that appears in Eq. (37) on the first line of Eq. (C1). This is because the order- $\alpha_s$   $\tilde{K}(b_*; \mu_b)$  vanishes exactly when a choice of  $C_1 = 2e^{-\gamma_E}$  is made. Note that the  $b_T$ -dependent part is linear in  $\ln Q$ .

The result for the Sun-Yuan formalism, Eq. (42), is

$$\begin{aligned} & -2C_F \int_{Q_0}^Q \frac{d\mu'}{\mu'} \frac{\alpha_s(\mu')}{\pi} \left[ \ln \left( \frac{Q^2}{\mu'^2} \right) + \ln \left( \frac{Q_0^2 b_T^2}{C_1^2} \right) - \frac{3}{2} \right] \\ &= -\frac{4A}{3\pi} \left[ 2 \ln(Q/\Lambda_{QCD}) \ln \left( \frac{\ln(Q/\Lambda_{QCD})}{\ln(Q_0/\Lambda_{QCD})} \right) - 2 \ln(Q/Q_0) + \left( \ln \left( \frac{Q_0^2 b_T^2}{C_1^2} \right) - \frac{3}{2} \right) \ln \left( \frac{\ln(Q/\Lambda_{QCD})}{\ln(Q_0/\Lambda_{QCD})} \right) \right]. \end{aligned} \quad (\text{C2})$$

### Acknowledgments

T. Rogers is supported by the National Science Foundation, grant PHY-0969739, and L. Gamberg is supported by the U.S. Department of Energy under grant No. DE-FG02-07ER41460. T. Rogers thanks Christian Weiss for discussions that helped lead to the formulation of this project. We especially thank the COMPASS collaboration, particularly Andrea Bressan, for discussions. We thank John Collins, Mariaelena Boglione, Zhongbo Kang, Pavel Nadolsky, Alexei Prokudin, Andrea Signori, George Sterman, and Mark Strikman for helpful discussions.

- 
- [1] *Gluons and the quark sea at high energies: Distributions, polarization, tomography* (2011), 1108.1713.
  - [2] I. Balitsky, A. Prokudin, and A. Radyushkin, eds., *Proceedings of QCD Evolution Workshop on From Collinear to Non-Collinear Case*, vol. 04 (2011).
  - [3] J. C. Collins, *Foundations of Perturbative QCD* (Cambridge University Press, Cambridge, 2011).
  - [4] D. W. Sivers, Phys. Rev. **D41**, 83 (1990).
  - [5] J. C. Collins, Phys. Lett. **B536**, 43 (2002), hep-ph/0204004.
  - [6] J. C. Collins and D. E. Soper, Nucl.Phys. **B193**, 381 (1981).
  - [7] J. C. Collins and D. E. Soper, Nucl.Phys. **B194**, 445 (1982).
  - [8] J. C. Collins, D. E. Soper, and G. F. Sterman, Nucl.Phys. **B250**, 199 (1985).
  - [9] G. Ladinsky and C. Yuan, Phys.Rev. **D50**, 4239 (1994), hep-ph/9311341.
  - [10] C. Balazs, J.-w. Qiu, and C. Yuan, Phys.Lett. **B355**, 548 (1995), hep-ph/9505203.
  - [11] C. Balazs and C. Yuan, Phys.Rev.Lett. **79**, 2398 (1997), hep-ph/9703405.
  - [12] C. Balazs and C. Yuan, Phys.Rev. **D56**, 5558 (1997), hep-ph/9704258.
  - [13] C.P.-Yuan, *Q<sub>T</sub> resummation portal*, URL <http://hep.pa.msu.edu/resum/>.
  - [14] R. Meng, F. I. Olness, and D. E. Soper, Phys. Rev. **D54**, 1919 (1996), hep-ph/9511311.

- [15] P. M. Nadolsky, D. Stump, and C. Yuan, Phys.Rev. **D61**, 014003 (2000), hep-ph/9906280.
- [16] P. M. Nadolsky, D. Stump, and C. Yuan, Phys.Rev. **D64**, 114011 (2001), hep-ph/0012261.
- [17] J. C. Collins, Acta Phys. Polon. **B34**, 3103 (2003), hep-ph/0304122.
- [18] X.-d. Ji, J.-p. Ma, and F. Yuan, Phys. Rev. **D71**, 034005 (2005), hep-ph/0404183.
- [19] X.-d. Ji, J.-P. Ma, and F. Yuan, Phys. Lett. **B597**, 299 (2004), hep-ph/0405085.
- [20] M. G. Echevarria, A. Idilbi, and I. Scimemi, JHEP **1207**, 002 (2012), 1111.4996.
- [21] J. C. Collins and T. C. Rogers, Phys.Rev. **D87**, 034018 (2013), 1210.2100.
- [22] M. G. Echevarria, A. Idilbi, and I. Scimemi, Phys.Lett. **B726**, 795 (2013), 1211.1947.
- [23] V. Gribov and L. Lipatov, Sov.J.Nucl.Phys. **15**, 438 (1972).
- [24] G. Altarelli and G. Parisi, Nucl.Phys. **B126**, 298 (1977).
- [25] Y. L. Dokshitzer, Sov.Phys.JETP **46**, 641 (1977).
- [26] J. Collins (2012), 1212.5974.
- [27] W. Oliver, H. R. Gustafson, L. W. Jones, M. Longo, T. Roberts, et al., AIP Conf.Proc. **45**, 93 (1978).
- [28] E. Anassontzis, S. Katsanevas, E. Kiritsis, P. Kostarakis, C. Kourkoumelis, et al., Phys.Rev. **D38**, 1377 (1988).
- [29] H. Reinhardt and R. Wunsch, Phys.Lett. **B215**, 577 (1988).
- [30] D. Diakonov, V. Y. Petrov, and P. Pobylitsa, Nucl.Phys. **B306**, 809 (1988).
- [31] C. Christov, A. Blotz, H.-C. Kim, P. Pobylitsa, T. Watabe, et al., Prog.Part.Nucl.Phys. **37**, 91 (1996), hep-ph/9604441.
- [32] H. Weigel, Lect.Notes Phys. **743**, 1 (2008).
- [33] M. Wakamatsu, Phys.Rev. **D79**, 014033 (2009), 0811.4196.
- [34] P. Schweitzer, M. Strikman, and C. Weiss, JHEP **1301**, 163 (2013), 1210.1267.
- [35] P. Schweitzer, M. Strikman, and C. Weiss, Acta Phys.Polon.Supp. **6**, 109 (2013), 1212.4031.
- [36] A. Airapetian et al. (HERMES Collaboration), Phys.Rev. **D87**, 074029 (2013), 1212.5407.
- [37] A. Signori, A. Bacchetta, M. Radici, and G. Schnell, JHEP **1311**, 194 (2013), 1309.3507.
- [38] M. Anselmino, M. Boglione, J. O. Gonzalez H., S. Melis, and A. Prokudin (2013), 1312.6261.
- [39] A. Airapetian et al. (HERMES Collaboration), Phys.Lett. **B684**, 114 (2010), 0906.2478.
- [40] C. Adolph et al. (COMPASS), Eur.Phys.J. **C73**, 2531 (2013), 1305.7317.
- [41] R. Seidl et al. (Belle), Phys. Rev. **D78**, 032011 (2008), 0805.2975.
- [42] D. Boer, Nucl.Phys. **B806**, 23 (2009), 0804.2408.
- [43] F. Landry, R. Brock, P. M. Nadolsky, and C. P. Yuan, Phys. Rev. **D67**, 073016 (2003), hep-ph/0212159.
- [44] A. V. Konychev and P. M. Nadolsky, Phys.Lett. **B633**, 710 (2006), hep-ph/0506225.
- [45] M. Guzzi, P. M. Nadolsky, and B. Wang (2013), 1309.1393.
- [46] P. M. Nadolsky, AIP Conf.Proc. **753**, 158 (2005), hep-ph/0412146.
- [47] R. Lopes de Sa, Ph.D. thesis, Stony Brook University (2013).
- [48] M. G. Echevarria, A. Idilbi, A. Schafer, and I. Scimemi, Eur.Phys.J. **C73**, 2636 (2013), 1208.1281.
- [49] P. Sun and F. Yuan, Phys.Rev. **D88**, 034016 (2013), 1304.5037.
- [50] P. Sun and F. Yuan, Phys.Rev. **D88**, 114012 (2013), 1308.5003.
- [51] A. Bacchetta, D. Boer, M. Diehl, and P. J. Mulders, JHEP **08**, 023 (2008), 0803.0227.
- [52] J. Collins (2013), 1307.2920.
- [53] G. P. Korchemsky and G. F. Sterman, Nucl.Phys. **B437**, 415 (1995), hep-ph/9411211.
- [54] S. Tafat, JHEP **0105**, 004 (2001), hep-ph/0102237.
- [55] E. Laenen, G. F. Sterman, and W. Vogelsang, Phys.Rev. **D63**, 114018 (2001), hep-ph/0010080.
- [56] E. Laenen, G. F. Sterman, and W. Vogelsang, pp. 1411–1413 (2000), hep-ph/0010183.
- [57] D. Boer, Nucl.Phys. **B603**, 195 (2001), hep-ph/0102071.
- [58] S. M. Aybat and T. C. Rogers, Phys. Rev. **D83**, 114042 (2011), 1101.5057.
- [59] P. Schweitzer, T. Teckentrup, and A. Metz, Phys.Rev. **D81**, 094019 (2010), 1003.2190.
- [60] J.-w. Qiu and X.-f. Zhang, Phys.Rev. **D63**, 114011 (2001), hep-ph/0012348.
- [61] S. M. Aybat, J. C. Collins, J.-W. Qiu, and T. C. Rogers (2011), 1110.6428.
- [62] S. M. Aybat, A. Prokudin, and T. C. Rogers, Phys.Rev.Lett. **108**, 242003 (2012), 1112.4423.
- [63] D. Boer, Nucl.Phys. **B874**, 217 (2013), 1304.5387.
- [64] A. Signori, S. M. Aybat, A. Prokudin, and T. C. Rogers, *TMD project*, URL <http://projects.hepforge.org/tmd/>.
- [65] G. Parisi and R. Petronzio, Nucl.Phys. **B154**, 427 (1979).
- [66] J.-w. Qiu and X.-f. Zhang (2002), hep-ph/0205115.
- [67] E. V. Shuryak, Nucl.Phys. **B203**, 93 (1982).
- [68] D. Diakonov and V. Y. Petrov, Nucl.Phys. **B272**, 457 (1986).
- [69] T. Schaefer and E. V. Shuryak, Rev.Mod.Phys. **70**, 323 (1998), hep-ph/9610451.
- [70] M. V. Polyakov and C. Weiss, Phys.Lett. **B387**, 841 (1996), hep-ph/9607244.
- [71] J. Beringer et al. (Particle Data Group), Phys.Rev. **D86**, 010001 (2012).
- [72] R. Bhaduri, *Models of the Nucleon: From Quarks to Soliton* (ADDISON-WESLEY, Redwood City, USA, 1988).
- [73] F. Yuan, Phys.Lett. **B575**, 45 (2003), hep-ph/0308157.
- [74] A. Courtoy, S. Scopetta, and V. Vento, Phys.Rev. **D79**, 074001 (2009), 0811.1191.
- [75] R. E. Walpole, R. H. Myers, S. L. Myers, and K. E. Ye, *Probability and Statistics for Engineers and Scientists (9th Edition)*, 9th (Pearson, January 6, 2011).
- [76] J. C. Collins and T. Rogers, in preparation (2013).
- [77] J. Collins, T. Rogers, and A. Stasto, Phys.Rev. **D77**, 085009 (2008), 0708.2833.



- [78] J.-C. Peng and J.-W. Qiu (2014), 1401.0934.
- [79] S. Bethke, Eur.Phys.J. **C64**, 689 (2009), 0908.1135.